Helsinki University of Technology Control Engineering
Espoo 2009
Report 163

REFLECTANCE SPECTRUM ANALYSIS OF MINERAL FLOTATION FROTHS AND SLURRIES

Olli Haavisto

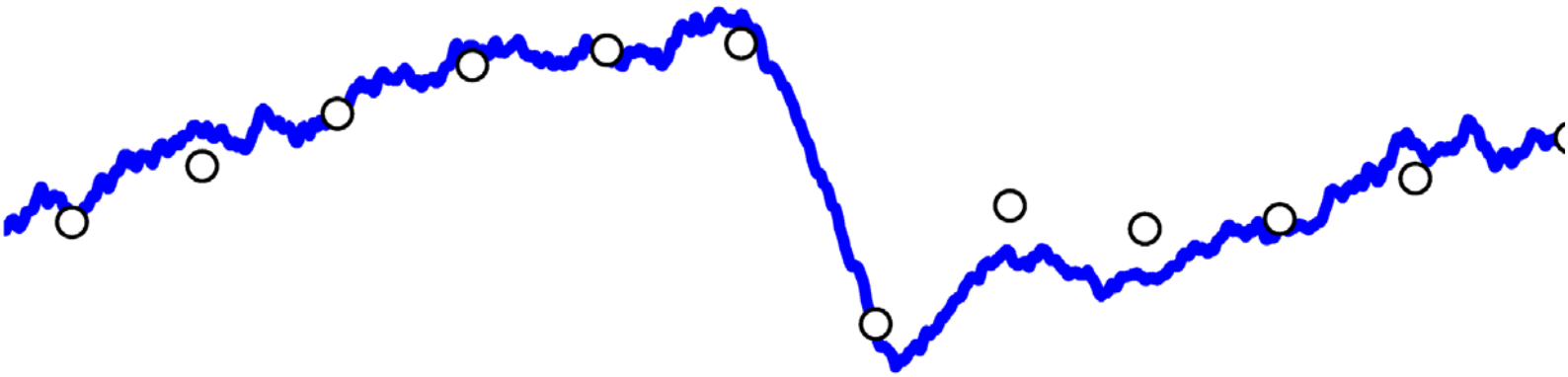

TEKNILLINEN KORKEAKOULU
TEKNISKA HÖGSKOLAN
HELSINKI UNIVERSITY OF TECHNOLOGY
TECHNISCHE UNIVERSITÄT HELSINKI
UNIVERSITE DE TECHNOLOGIE D'HELSINKI

Helsinki University of Technology Control Engineering

Espoo November 2009 Report 163

REFLECTANCE SPECTRUM ANALYSIS OF MINERAL FLOTATION FROTHS AND SLURRIES

Olli Haavisto

Dissertation for the degree of Doctor of Science in Technology to be presented with due permission of the Faculty of Electronics, Communications and Automation, for public examination and debate in Auditorium AS1 at Helsinki University of Technology (Espoo, Finland) on the 11th of December, 2009, at 12 noon.

Helsinki University of Technology

Faculty of Electronics, Communications and Automation

Department of Automation and Systems Technology

Distribution:
Helsinki University of Technology
Department of Automation and Systems Technology
P.O. Box 5500
FI-02015 TKK, Finland
Tel. +358-9-470 25201
Fax. +358-9-470 25208
E-mail: control.engineering@tkk.fi
http://autsys.tkk.fi/

ISBN 978-952-248-236-5 (printed)
ISBN 978-952-248-237-2 (pdf)
ISSN 0356-0872

Yliopistopaino
Helsinki 2009

Available on net at http://lib.tkk.fi/Diss/2009/isbn9789522482372

ABSTRACT OF DOCTORAL DISSERTATION	HELSINKI UNIVERSITY OF TECHNOLOGY P.O. BOX 1000, FI-02015 TKK http://www.tkk.fi

Author Olli Haavisto

Name of the dissertation
Reflectance Spectrum Analysis of Mineral Flotation Froths and Slurries

Manuscript submitted September 9, 2009	Manuscript revised November 16, 2009
Date of the defence December 11, 2009	
☐ Monograph	☒ Article dissertation (summary + original articles)

Faculty	Faculty of Electronics, Communications and Automation
Department	Department of Automation and Systems Technology
Field of research	Control Engineering
Opponent(s)	Prof. John Meech, Prof. Robert Piché
Supervisor	Prof. Heikki Koivo
Instructor	Prof. Heikki Hyötyniemi

Abstract

The global demand of mining products has increased during recent years, and there is pressure to improve the efficiency of mines and concentration processes. This thesis focuses on froth flotation, which is one of the most common concentration methods in mineral engineering. Froth flotation is used to separate valuable minerals from mined ore that has been crushed, mixed with water and ground to a small particle size. The separation is based on differences in the surface chemical properties of the minerals. Monitoring and control of flotation processes mainly relies on the on-line analysis of the process slurry streams. Traditionally, the analysis is performed using X-ray fluorescence (XRF) analyzers that measure the elemental contents of the solids in the slurries.

The thesis investigates the application of visual and near-infrared (VNIR) reflectance spectroscopy to improve the on-line analysis of mineral flotation froths and slurries. In reflectance spectroscopy the sample is illuminated and the spectrum of the reflected light is captured by a spectrograph. The main benefits of VNIR reflectance spectroscopy with respect to XRF-based analysis are the relatively low cost of the equipment required and the easy and fast measurement process. As a consequence, the sampling rate of the reflectance spectrum measurement is radically faster than in the XRF analysis. Data-based modeling is applied to the measured VNIR spectra to calculate the corresponding elemental contents. The research is conducted at a real copper and zinc flotation process.

The main results of the thesis show that VNIR reflectance spectroscopy can be used to measure temporal changes in the elemental contents of mineral flotation froths and slurries in the analyzed process. Especially the slurry measurements from the final concentrates provide accurate information on the slurry contents. A multi-channel slurry VNIR analyzer prototype is developed in this thesis. When combined with an XRF analyzer, it is able to measure the slurry lines with a very fast sampling rate. This considerably improves the monitoring and control possibilities of the flotation process. The proposed VNIR analyzer is adaptively calibrated with the sparse XRF measurements to compensate for the effect of changes in other slurry properties. The high-frequency slurry analysis is shown to reveal fast grade changes and grade oscillations that the XRF analyzer is unable to detect alone. Based on the new measurement, a plant-wide study of the harmful grade oscillations is conducted in order to improve the performance of the flotation process.

Keywords Froth flotation, mineral concentration, reflectance spectroscopy, data-based modeling, X-ray fluorescence

ISBN (printed)	978-952-248-236-5	ISSN (printed)	0356-0872
ISBN (pdf)	978-952-248-237-2	ISSN (pdf)	
Language	English	Number of pages	74 + 66

Publisher Helsinki University of Technology, Department of Automation and Systems Technology

Print distribution Helsinki University of Technology, Department of Automation and Systems Technology

☒ The dissertation can be read at http://lib.tkk.fi/Diss/2009/isbn9789522482372/

VÄITÖSKIRJAN TIIVISTELMÄ	TEKNILLINEN KORKEAKOULU PL 1000, 02015 TKK http://www.tkk.fi

Tekijä Olli Haavisto

Väitöskirjan nimi
Mineraalivaahdotuksen vaahtojen ja lietteiden heijastusspektrianalyysi

Käsikirjoituksen päivämäärä 9.9.2009	Korjatun käsikirjoituksen päivämäärä 16.11.2009
Väitöstilaisuuden ajankohta 11.12.2009	
☐ Monografia	☒ Yhdistelmäväitöskirja (yhteenveto + erillisartikkelit)

Tiedekunta	Elektroniikan, tietoliikenteen ja automaation tiedekunta
Laitos	Automaatio- ja systeemitekniikan laitos
Tutkimusala	Systeemitekniikka
Vastaväittäjä(t)	Prof. John Meech, Prof. Robert Piché
Työn valvoja	Prof. Heikki Koivo
Työn ohjaaja	Prof. Heikki Hyötyniemi

Tiivistelmä

Kaivosteollisuuden tuotteiden kansainvälinen kysyntä on lisääntynyt viimeisten vuosien aikana, minkä seurauksena kaivokset ja rikastamot pyrkivät nostamaan suorituskykyään. Väitöskirjassa keskitytään vaahdotusrikastukseen, joka on yksi yleisimmistä rikastusmenetelmistä. Vaahdotuksessa murskatusta ja veteen sekoitettuna hienoksi jauhetusta malmista erotetaan arvomineraalit hyödyntäen eroja mineraalien pintakemiallisissa ominaisuuksissa. Vaahdotusprosessin monitorointi ja säätö perustuu pääosin prosessin lietevirtausten on-line-pitoisuusanalyysiin. Perinteisesti pitoisuusanalyysiin käytetään röntgenfluoresenssianalysaattoreita, jotka mittaavat lietteen kiintoaineen alkuainepitoisuuksia.

Väitöskirjassa tutkitaan näkyvän ja lähi-infrapuna-alueen heijastusspektroskopian soveltamista mineraalivaahdotuksen vaahtojen ja lietteiden pitoisuusmittausten parantamiseen. Heijastusspektroskopiassa näyte valaistaan ja heijastuneen valon spektri mitataan spektrometrillä. Heijastusspektroskopian tärkeimmät edut röntgenfluoresenssiin perustuvaan analyysiin verrattuna ovat tarvittavan laitteiston suhteellinen edullisuus sekä mittauksen helppous ja nopeus. Tästä johtuen reflektanssispektrimittauksen mittaustaajuus pystytään nostamaan huomattavasti korkeammaksi kuin röntgenfluoresenssianalyysissä. Lietteen alkuainepitoisuusarvot lasketaan mitatusta spektridatasta datapohjaisilla mallitusmenetelmillä. Tutkimus keskittyy todellisen kupari- ja sinkkivaahdotusprosessin lietevirtausten analysointiin.

Väitöskirjan päätuloksena osoitetaan, että näkyvän ja lähi-infrapuna-alueen heijastusspektroskopia soveltuu mineraalivaahdotuksen vaahtojen ja lietteiden alkuainepitoisuuksien vaihteluiden mittaamiseen tarkasteltavassa prosessissa. Varsinkin rikastelietteistä mitatuista spektreistä pystytään tarkasti laskemaan vastaavat pitoisuudet. Väitöskirjassa kehitetään monikanavainen prototyyppilaitteisto, joka mittaa lietteen heijastusspektrin ja yhdistettynä röntgenfluoresenssianalysaattoriin analysoi lietelinjan pitoisuudet hyvin korkealla näytteenottotaajuudella. Tämä parantaa merkittävästi vaahdotusprosessin monitorointi- ja säätömahdollisuuksia. Lietteen ominaisuuksien vaihteluiden vaikutukset analyysiin eliminoidaan kalibroimalla pitoisuuslaskentaa harvoilla röntgenfluoresenssimittauksilla. Työssä osoitetaan, että korkeataajuisesta heijastusspektrianalyysistä voidaan havaita sellaisetkin nopeat pitoisuusmuutokset ja värähtelyt, joita pelkällä röntgenfluoresenssianalysaattorilla ei pystytä mittaamaan. Uutta pitoisuusmittausta sovelletaan työssä myös koko prosessin kattavaan haitallisten värähtelyiden analyysiin, jonka tavoitteena on prosessin suorituskyvyn parantaminen.

Asiasanat Vaahdotus, mineraalien rikastus, reflektanssispektroskopia, datapohjainen mallinnus, röntgenfluoresenssi

ISBN (painettu)	978-952-248-236-5	ISSN (painettu)	0356-0872
ISBN (pdf)	978-952-248-237-2	ISSN (pdf)	
Kieli	Englanti	Sivumäärä	74 + 66
Julkaisija	Teknillinen korkeakoulu, Automaatio- ja systeemitekniikan laitos		
Painetun väitöskirjan jakelu	Teknillinen korkeakoulu, Automaatio- ja systeemitekniikan laitos		

☒ Luettavissa verkossa osoitteessa http://lib.tkk.fi/Diss/2009/isbn9789522482372/

A thesis can be considered a success if, after finishing it, the author knows how it should have been done.

Preface

This thesis summarizes the research that I have carried out in the Control Engineering Research Group (former Control Engineering Laboratory) of Helsinki University of Technology (TKK) during 2005–2009.

The thesis, as well as my earlier research work, was done under the guidance of Professor Heikki Hyötyniemi, to whom I would like to express my sincere gratitude. He kept me on my toes with his theory on complex systems and neocybernetics — all the way from the sieving of gold nuggets to the structure of the universe. I often left his office with more questions than I had when going in, which, considering the better quality of the questions I got in change, was very well worth it. Heikki's incredibly positive attitude and trust in my work was a constant source of encouragement during the thesis process.

Professor Heikki Koivo, the supervisor of the thesis, had an important role as the head of the research group and as the responsible leader of the projects I was working for. He deserves a special thanks for creating and maintaining an open and inspiring working atmosphere.

Main part of the actual research work was done in close collaboration with Dr. Jani Kaartinen, who – besides acting as the project manager – skillfully arranged most of the practical details related to the measurement prototypes and data gathering. I sincerely thank him, because without his contribution this thesis would not have been possible. I would also like to acknowledge the efforts of Janne Pietilä, Timo Roine and all the other colleagues with whom I have had the pleasure to work. I thank the rest of the staff of the research group for the good company particularly during lunch and coffee breaks.

The pre-examination of the thesis manuscript was performed by Professor Emeritus Raimo Ylinen (University of Oulu) and Professor John Meech (University of British Columbia). Their valuable comments and corrections are highly appreciated. In addition, William Martin from the Faculty of Electronics, Communications and Automation is acknowledged for the fast proof-reading of the manuscript.

The industrial collaboration with Pyhäsalmi Mine Oy and Outotec Minerals Oy was an essential part of the research. I am deeply grateful to Seppo Lähteenmäki, Jorma Miettunen, Aki Tuikka, Jarmo Huuskonen and other staff of Pyhäsalmi Mine as well as to Dr. Kari Saloheimo, Matti Kongas and other personnel of Outotec Minerals for providing us with the opportunity to use the Pyhäsalmi flotation process as a test case, for expert comments, for active participation in the prototype development and, above all, for the overall positive attitude towards the research. The

interest and encouraging feedback of the industrial partners were an important source of motivation throughout the years.

The thesis was mainly funded by the Graduate School in Electronics, Telecommunications and Automation (GETA), and by two TEKES projects. Additional financial support was received from Finnish Foundation for Technology Promotion, Neles Foundation, Walter Ahlström Foundation and Automation Foundation, whose generosity is also gratefully acknowledged.

In spring 2008 I had a wonderful opportunity to visit University of British Columbia in Vancouver, Canada, for almost three months. I thank Prof. John Meech from the Norman B. Keevil Institute of Mining Engineering at UBC for kindly arranging my stay and for introducing me to the research of the institute.

Finally, I would like to thank my parents and brother for their indirect but important support on the thesis work.

Olli Haavisto

Contents

Abbreviations

CAD	Computer aided design
CCD	Charge-coupled device
CEC	Cation exchange capacity
CLWR	Continuous locally weighted regression
FFT	Fast fourier transform
FIR	Far-infrared
IR	Infrared
K-M	Kubelka-Munk
K-OPLS	Kernel-based orthogonal projections to latent structures
LS	Least squares
LWIR	Long-wavelength infrared
LWPR	Locally weighted projection regression
LWR	Locally weighted regression
MIA	Multivariate image analysis
MSC	Multiplicative scatter correction
MSE	Mean square error
MWIR	Mid-wavelength infrared
NIPALS	Nonlinear iterative partial least squares
NIR	Near-infrared
O-PLS	Orthogonal projections to latent structures
OSC	Orthogonal signal correction
PC	Principal component
PCA	Principal component analysis
PCR	Principal component regression
PGP	Prism-grating-prism
PLS	Partial least squares
PLS-DA	Partial least squares discriminant analysis
RGB	Red, green and blue (color space)
rLS	Recursive least squares
rMM	Recursive multimodel algorithm
RMSE	Root mean square error
rPCA	Recursive principal component analysis
rPCR	Recursive principal component regression
rPLS	Recursive partial least squares
rSSA	Recursive singular spectrum analysis

SNV	Standard normal variate
SSA	Singular spectrum analysis
SVD	Singular value decomposition
SWIR	Short-wavelength infrared
UV	Ultraviolet
VIS	Visible
VNIR	Visible and near-infrared
XRD	X-ray diffraction
XRF	X-ray fluorescence

Nomenclature

The notation used in the compendium:

x, X	Scalars
$\boldsymbol{x}$	Column vector
$\boldsymbol{X}$	Matrix
$\boldsymbol{X}^T$	Transpose (of $\boldsymbol{X}$)
$\boldsymbol{X}^{-1}$	Inverse (of $\boldsymbol{X}$)
$\hat{x}$	Estimate (of x)

The list of symbols used in the compendium:

a	Molar absorptivity
A	Absorbance
b	Sample thickness
$\boldsymbol{b}$	Regression mapping for a single response variable
$\boldsymbol{B}$	Multivariate regression mapping matrix
c	Concentration
$\boldsymbol{C}$	PLS response weight matrix
d	Variable describing the rank of a matrix
$\boldsymbol{e}$	Regression error vector
$\boldsymbol{E}$	Regression error matrix
$E(\cdot)$	Expectation
$f(R)$	Kubelka-Munk function
$f(x_1, \ldots, x_n)$	Probability distribution function
$\boldsymbol{F}$	PLS residual matrix
$\boldsymbol{g}$	Time series vector for SSA
$\boldsymbol{G}$	PLS residual matrix
i	Index variable
I, I_0, I_R, I_T	Intensity of light (0=incident, R=reflected and T=transmitted)
k	Absorption coefficient, discrete time/sample index
K	Number of lagged vectors in SSA
l	Number of latent variables
L	SSA window length
m	Response data dimension
n	Predictor data dimension
N	Number of data samples
N_local	Number of local models

p	Number of SSA components used in reconstruction
$\boldsymbol{p}$	Loading vector
$\boldsymbol{P}$	Loading matrix
Q^2	Coefficient of determination (validation data)
$r_{X_iX_j}$	Covariance (of X_i and X_j)
R	Reflectance
R^2	Coefficient of determination (estimation data)
$\boldsymbol{R}_x$	Covariance matrix (of $\boldsymbol{x}$)
$\boldsymbol{R}_{xy}$	Cross-covariance matrix (of $\boldsymbol{x}$ and $\boldsymbol{y}$)
$\overline{\boldsymbol{R}}_x$	Unscaled covariance matrix (of $\boldsymbol{x}$)
s	Scattering coefficient
T	Transmittance
T_0	Memory time constant
$\boldsymbol{t}$	Score vector
$\boldsymbol{T}$	Score matrix
$\boldsymbol{w}^*$	PLS predictor weight vector
$\boldsymbol{W}^*$	PLS predictor weight matrix
X	Random variable
$\boldsymbol{x}$	Predictor sample vector
$\tilde{\boldsymbol{x}}$	Augmented predictor sample vector
$\boldsymbol{X}$	Predictor data matrix
$\boldsymbol{y}$	Response sample vector
$\boldsymbol{Y}$	Response data matrix
$\boldsymbol{z}$	Lagged vector in SSA
$\boldsymbol{Z}$	SSA trajectory matrix
γ	Gain used in the recursive weighted average algorithm
λ	Forgetting factor
λ_i	Variance of the i:th principal component
$\boldsymbol{\Lambda}$	Diagonal matrix of the principal component variances
μ_X	Mean (of X)
σ_X^2	Variance (of X)

List of Publications

I O. Haavisto, J. Kaartinen, and H. Hyötyniemi. Optical spectrum based estimation of grades in mineral flotation. In *Proceedings of the IEEE International Conference on Industrial Technology* (ICIT 2006), pp. 2529–2534, Mumbai, India, December 2006.

II O. Haavisto, J. Kaartinen, and H. Hyötyniemi. Optical spectrum based measurement of flotation slurry contents. *International Journal of Mineral Processing*, vol. 88, issues 3–4, pp. 80–88, 2008.

III O. Haavisto and H. Hyötyniemi. Partial least squares estimation of mineral flotation slurry contents using optical reflectance spectra. In *CAC 2008 - 11th International Conference on Chemometrics in Analytical Chemistry*, vol. 2 (Process Analysis), pp. 81–85, Montpellier, France, June–July 2008.

IV O. Haavisto and H. Hyötyniemi. Recursive multimodel partial least squares estimation of mineral flotation slurry contents using optical reflectance spectra. *Analytica Chimica Acta*, vol. 642, issues 1–2, pp. 102–109, 2009.

V O. Haavisto and J. Kaartinen. Multichannel reflectance spectral assaying of zinc and copper flotation slurries. *International Journal of Mineral Processing*, vol. 93, issue 2, pp. 187–193, 2009.

VI O. Haavisto. Detection and analysis of oscillations in a mineral flotation circuit, *Control Engineering Practice*, vol. 18, issue 1, pp. 23–30, 2010.

VII O. Haavisto and H. Hyötyniemi. Reflectance spectroscopy in the analysis of mineral flotation slurries. In *Pre-Prints of the Workshop on Automation in Mining, Mineral and Metal Industry* (IFACMMM2009), 6 pages, Viña del Mar, Chile, October 2009.

Chapter 1

Introduction

The worldwide demand for mining products peaked during the years 2006–2008, causing the metal and ore prices to rise accordingly. As a result, mineral deposits with poorer ores became economically feasible as well. New mining operations were planned and the operation of old ones could be extended by exploiting the existing ore reserves more carefully. The current economic recession, however, affected drastically the consumption and prices, which together with the lower grade ores emphasizes the importance of the concentration process performance. At the same time, tightened environmental requirements encourage the operations to strive for better sustainability. In concentration plants utilizing froth flotation, which is one of the most typical ore beneficiation methods, the more effective operation generally means that less valuable minerals are allowed in the tailings and the concentrate grade should be maximized, whereas the consumption of flotation chemicals and energy should be minimized.

1.1 Background and Motivation

The on-line analysis or assaying of the process streams in a flotation circuit forms the basis for process monitoring and control as well as for the evaluation of the concentration performance at the plant (McKee, 1991; Wills and Napier-Munn, 2006). On-line process analyzers utilizing X-ray fluorescence (XRF) have traditionally been used for assaying the streams particularly in base metal mineral processing (Braden et al., 2002; Cooper, 1976). The analysis is based on the measurement of the characteristic fluorescent radiation emitted by different elements when excited with high-energy X-ray radiation. However, the sequential measurement of several slurry lines by the same device and the time taken by the XRF analysis have restricted the sampling rate of the analysis especially in larger flotation plants that process complex ores.

Flotation froth structure and color analysis by machine vision has been widely studied as a supplemental method for analyzing the state of flotation cells (see e.g. Bartolacci et al., 2006; Kaartinen et al., 2006b; Liu and MacGregor, 2008; Morar et al., 2005). It is generally accepted that froth color and mineral grade correlate in certain flotation processes. However, there are very few real process applications

where the color information had been used for analyzing the grade of froths or slurries. Instead, other froth characteristics like froth speed and bubble size have proven to be more reliable and useful variables for process monitoring and control purposes.

The measurement of color in general has recently been improved by the development of devices in the field of reflectance spectroscopy. Especially the properties of imaging spectrographs capable of hyperspectral imaging in visible and near-infrared wavelengths have significantly developed during the last decade. Some of the new possibilities enabled by these devices are utilized in this thesis.

1.2 Objectives and Scope of the Thesis

The thesis considers the reflectance spectral analysis of mineral flotation froths and slurries. The main objective is to evaluate the usefulness of the color information for analyzing the elemental contents of the slurries, and to apply the improved grade measurements to flotation process monitoring and control. The primary improvement aimed for is the shortening of the presently rather long sampling interval of a typical XRF analyzer.

The emphasis of the research is on the development of techniques for the on-line analysis of real flotation process streams instead of extensive laboratory testing or deep theoretical discussions. For this purpose, the measurements are mainly conducted at an operating concentration plant (Pyhäsalmi mine, Inmet Mining Corporation). The analysis is restricted to the copper-zinc ore processed at the plant. However, all the developed measurement devices and data processing methods can readily be generalized to other flotation processes, and the presented results can be used to evaluate the suitability of the approach to other ore types.

The spectral measurements in this thesis cover the visible and near-infrared (VNIR) range (400–1000 nm), which is a necessary restriction in order to maintain the low cost of the measurement instruments. The results of the on-line XRF analyzer at the plant are utilized as reference values for both calibrating and validating the reflectance spectral measurements.

Data-based modeling has an important role throughout the whole thesis, and special effort is put into the proper selection of the most suitable calibration methods. The data modeling challenges stem on one hand from the generally difficult interpretability of reflectance spectra, and on the other hand from the varying and unpredictable behavior of flotation slurry properties. As a way of dealing with these issues, recursive modeling is intensively utilized.

1.3 Contributions of the Thesis

The main contribution of this thesis is the combination of VNIR reflectance spectroscopy with XRF analysis in order to create a novel and improved method for assaying mineral flotation froths and slurries. More specifically, the thesis contains the following contributions:

- Froth analysis
  - comparison of the RGB color and VNIR reflectance spectral measurements for assaying the final zinc concentrate froth (Publication **I**)
  - first reported application of VNIR reflectance spectroscopy for increasing the sampling rate of an XRF analyzer (Publication **I**)
  - comparison of the properties of zinc concentrate froth and slurry reflectance spectra (Publication **I**)
- Slurry analysis
  - first real process environment results showing the good precision of the VNIR reflectance spectral assaying in the final zinc concentrate slurry (Publication **II**) and in the final copper concentrate (Publication **V**)
  - evaluation of the VNIR slurry analysis performance in the other main zinc and copper flotation slurries (Publication **V**)
  - significant improvement in the assaying of final zinc concentrate (Publication **II**) and final copper concentrate (Publication **V**) by combining VNIR reflectance spectral measurements with the XRF analysis
  - novel analysis of the high-frequency properties of the final concentrate grades based on the developed high-frequency VNIR slurry assay (Publications **II** and **V**)
  - evaluation of the error distribution parameters of the high-frequency VNIR assay with respect to XRF (Publication **VII**)
  - plant-wide oscillation analysis of the copper flotation circuit based on the high-frequency VNIR assay (Publication **VI**)
- Algorithm development
  - two novel recursive local modeling algorithms for capturing rare process failures (Publications **III** and **IV**)
  - new orthogonal signal correction (OSC) kernel algorithm (Publication **IV**)
  - new on-line algorithm for plant-wide oscillation detection and analysis in general industrial processes (Publication **VI**)

1.4 Publications

The thesis consists of seven publications (appended to the end). This section summarizes their contents and lists the author's contributions.

1.4.1 Summaries

Publication I The determination of mineral froth grades based on the VNIR reflectance spectrum of the final zinc concentrate froth at the Pyhäsalmi concentration

plant is studied in this publication. A partial least squares (PLS) model is estimated from XRF and VNIR spectrum data to predict the elemental contents from the spectra. The results indicate that the VNIR spectra give slightly better elemental grade estimates for copper, zinc and iron than the RGB color data used for comparison. Based on the results, the reflectance spectrum measurement is suggested as a complementary method to improve the sparse XRF assays with more frequent data. Initial laboratory results for the final zinc concentrate slurry spectrum analysis are presented as well, referring to the possibility of even more accurate grade measurements directly from the spectra of the mineral slurries.

Publication II This article introduces the application of VNIR reflectance spectroscopy to the elemental assaying of mineral flotation slurries. Laboratory measurements are first presented to demonstrate that large grade differences are clearly seen in the VNIR spectra. The structure and installation of an on-line slurry spectrum analyzer prototype is then described. The measurement results from the final zinc concentrate slurry of the Pyhäsalmi concentration plant show that the main elemental grades of the slurry can be reliably predicted from the VNIR spectra. However, the PLS calibration model has to be recursively updated with the XRF assays to maintain a good prediction accuracy. The proposed method complements the XRF analyzer by reducing the sampling interval from around 15 minutes to ten seconds. This enables the detection of rapid changes and oscillations in the grades and thus substantially improves the process monitoring capabilities at the plant.

Publication III This article deals with the estimation of small elemental grades when using the slurry spectrum analysis developed in Publication II. Typically, the normally very small elemental grades in the concentrates increase significantly in the case of a process disturbance. The ordinary recursive PLS model is replaced in this article by a novel local modeling approach utilizing orthogonal signal correction (OSC) preprocessing and local PLS models. The developed modeling method is based on adaptively updated calibration database and on the ad hoc calculation of the PLS model. The performance of the modeling approach is demonstrated in the copper grade of the final zinc concentrate. It is shown that the developed method predicts the start of a new process failure with significantly better precision that the ordinary recursive PLS model.

Publication IV This publication addresses the same issue of sudden grade changes related to process failures as Publication **III**. The database of the previous approach is, however, replaced with pre-calculated but recursive local PLS models, which together cover the whole response data range. The benefits of the multimodel structure are a faster prediction calculation and a smaller memory consumption since no data points have to be stored. The developed algorithm is applied to the same copper grade data as in Publication **III**, and the results are compared to static and recursive PLS models. It is shown that the method is able to predict the critical first process failure value with clearly better precision than the other methods. Finally, the

high-frequency estimation of the copper grade is presented as a supplement for the ordinary XRF analyzer.

Publication V A multi-channel slurry VNIR spectrum analyzer is introduced in this publication. Based on the principles presented in Publication II, the analysis is extended to cover several slurry lines simultaneously. Seven slurry lines of the zinc and copper flotation circuits at Pyhäsalmi are analyzed. Large data sets of spectra and XRF assays are collected from all the lines and the shape of the spectra as well as the prediction precisions of the recursive PLS models are compared between the lines. The results show that the average VNIR spectrum mainly indicates the sphalerite/chalcopyrite (i.e. zinc/copper) ratio of the average grades in the slurry. Especially the copper and zinc concentrates with high sphalerite and chalcopyrite grades result in distinctive spectra. Accordingly, the best grade predictions are obtained from the two concentrates for the same reason. The high-frequency assay performance is demonstrated for these slurries as a method to detect oscillations and grade drops.

Publication VI This article presents the utilization of the high-frequency VNIR slurry analysis developed in Publications **II** and **V** for detecting oscillations in the Pyhäsalmi copper flotation circuit. For this purpose, a recursive extension of a data-based signal analysis method, singular spectrum analysis (SSA), is derived and applied to grade, flow rate and level signals of the circuit. The aim of the study is to detect and analyse the origins and spreading of the oscillations on-line in order to pinpoint the source and to eliminate it. This will improve the performance of the circuit. It is shown that the oscillations can be effectively detected by the proposed method and that the structural similarity between the oscillatory signal and the other process signals can be quantified in real time.

Publication VII The third slurry analyzer prototype with a more straightforward slurry sampling is described and utilized in this publication. The benefits of the high-frequency slurry assay are demonstrated for high- and low-frequency oscillations as well as for large grade changes in the zinc and copper concentrates. An on-line estimate for the VNIR assay error distribution with respect to the XRF values is presented. The estimate enables the evaluation of the assay confidence limits and the degradation rate of the estimate if no new XRF samples are available for calibration.

1.4.2 Author's Contributions

Publication I The author is responsible for the froth data modeling and results as well as the slurry data analysis. He also wrote the entire manuscript. Jani Kaartinen was in charge of the measurement arrangements and Prof. Heikki Hyötyniemi supervised the research. Both co-authors commented on the manuscript.

Publication II The author performed the modeling and analysis of the on-line data and produced the corresponding results. Jani Kaartinen is responsible for the measurements and results of the laboratory experiments as well as for the construction of the on-line slurry analyzer prototype. The author wrote the manuscript except for Sections 2.2-2.4 and 3.1, which were written by Kaartinen. Prof. Heikki Hyötyniemi supervised the research.

Publications III and IV The author is responsible for the contents of the publications and he wrote all the text. Prof. Heikki Hyötyniemi supervised the research and commented on the manuscripts.

Publication V The author is responsible for the analysis and modeling of the data as well as for the results obtained. The slurry analyzer prototype was designed in collaboration with Jani Kaartinen. The author wrote the whole manuscript except for Section 2.2 which was mainly contributed by Kaartinen.

Publication VI The author is solely responsible for the whole publication.

Publication VII The author is responsible for the contents of the publication and wrote the manuscript. Prof. Heikki Hyötyniemi commented on the manuscript and supervised the research.

1.5 Structure of the Thesis

This thesis is an article dissertation consisting of a compendium part and seven publications. The compendium can be divided into two major parts: Chapters 2–5 provide a concise literature survey in order to familiarize the reader with the background of the presented research, and Chapters 6–8 summarize and discuss the work originally presented in the publications. In more detail, Chapter 2 gives a short introduction to froth flotation in mineral processing, Chapter 3 deals with the basic concepts of reflectance spectroscopy, Chapter 4 surveys the literature published on the application of color and spectral measurements in mineral engineering, and Chapter 5 summarizes the data-based multivariate methods relevant to this work. The measurement arrangements and modeling methods used in the publications are presented in Chapter 6, whereas Chapter 7 discusses the results obtained. Finally, Chapter 8 concludes the whole research work.

Chapter 2

Froth Flotation in Mineral Processing

The purpose of mineral concentration is to separate valuable minerals from the gangue. The variety of concentration methods include froth flotation, gravity concentration and magnetic and electrical separation, among others. One of the most important methods is flotation: over 90% of base metals are concentrated using flotation (Matis and Zouboulis, 1995). Froth flotation was patented already in 1906, but still the very complex surface chemical mechanisms taking place in the flotation cells are not completely understood, even though a lot of research has been conducted on the subject (for recent studies, see e.g. Chau, 2009; Englert et al., 2009; Kracht and Finch, 2009).

The purpose of this chapter is to familiarize the reader with the basic concepts of froth flotation as a mineral processing method. Main emphasis is on the control aspects of flotation processes, and a concise introduction to the Pyhäsalmi process is presented as well. Several textbooks (e.g. Fuerstenau et al., 2007; Matis and Zouboulis, 1995; Rao, 2004) focusing on different aspects of flotation are available for more information.

2.1 Principle of Flotation

Froth flotation is the most important and versatile of the concentration methods since it can be applied to a wide variety of ores and particle sizes by selecting the correct flotation chemicals. The separation by flotation is based on the different surface chemical properties of the valuable and gangue mineral particles. Before the actual separation, mineral slurry is formed by grinding the ore with water. The slurry is then treated with flotation chemicals specific to the processed ore. The flotation chemicals can be divided into three main classes (Crozier, 1992): collectors attach to selected mineral particles and make them hydrophobic (i.e. water-repellant); frothers form and stabilize the froth layer; and finally modifiers, activators and depressants are used to balance the flotation environment and to enhance or subdue the floatability of specific minerals.

The treated slurry is processed in flotation cells (Figure 2.1) where air is pumped to the bottom of the cell and heavy mixing is applied. Because of the hydrophobic nature of the mineral particles to be separated, they attach to the rising air bubbles and are lifted to the surface of the cell. There the slurry forms a stable froth layer which can be skimmed or allowed to overflow from the cell. In direct flotation, valuable mineral particles are lifted to the froth and tailings are removed from the bottom of the cell, whereas in reverse flotation tailings are collected by the froth. A detailed description of the flotation cell operation principle and mechanical structure is given, for example, by Gorain et al. (2007).

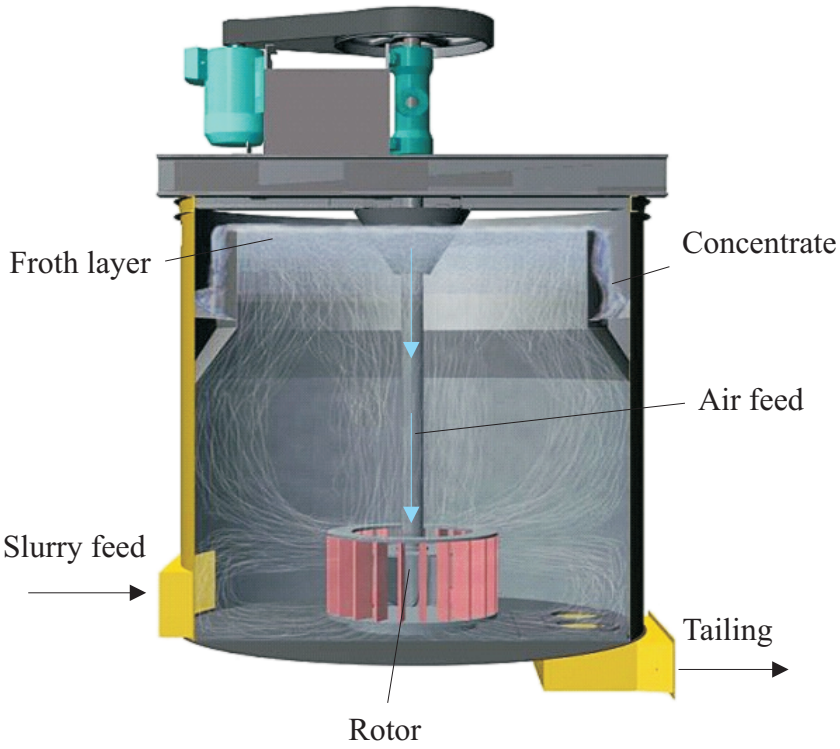

Figure 2.1: The basic structure of a froth flotation cell. (The CAD image Courtesy of Outotec Minerals Oy)

The separation achieved by a single flotation cell is usually not adequate to fulfill the final concentrate requirements. Consequently, typical flotation circuits consist of several interconnected flotation stages which contain several flotation cells each. The different flotation stages have specialized operating profiles and parameters. Possible flotation circuit flowsheet structures are discussed with more detail by Wills and Napier-Munn (2006), and as an example the structure of the Pyhäsalmi copper and zinc flotation circuits is presented in Section 2.3. The current flotation plant design principles have recently been reviewed by Mendez et al. (2009).

2.2 Control of a Flotation Process

Flotation circuits are traditionally considered as one of the most challenging industrial processes to control. This section briefly introduces the general control and monitoring issues faced in flotation plants. Especially the importance of the accurate on-line grade measurements (assays) of the flotation slurry streams is addressed as they are essential for control, process monitoring and circuit performance evaluation. The text is mainly based on the publications by McKee (1991) and Wills and Napier-Munn (2006).

2.2.1 Control Objectives

The metallurgical performance of a flotation process is determined by its capability to collect the valuable minerals from the incoming ore (i.e. recovery) as well as by the relative amount of the valuable mineral in the final product (i.e. grade). There is, however, a trade-off between these two properties since better recovery usually means lower grade and vice versa. Even though in reality the changing input ore properties constantly cause variations in the process, a theoretical steady state relationship between grade and recovery is often illustrated by a simple grade-recovery curve (Figure 2.2).

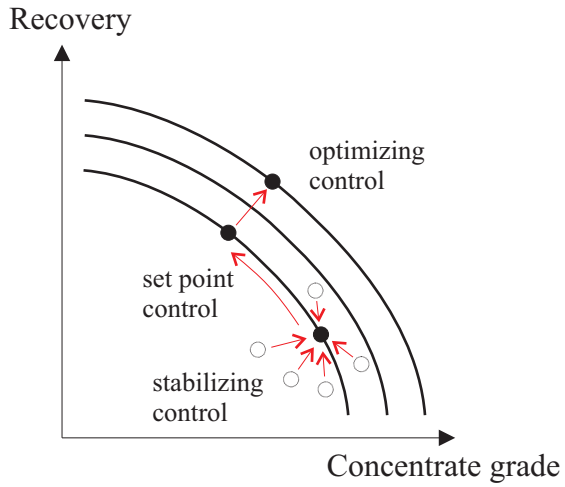

Figure 2.2: The trade-off between the concentrate grade and recovery of a flotation process as well as the different control objectives. (Modified from Wills and Napier-Munn, 2006)

It is generally accepted that the starting point in flotation circuit control is to stabilize the operation of the process. This involves the stabilization of the slurry levels in the flotation cells and pump sumps as well as the regulation of air and reagent flows. After that, the target should be to reach the desired operating point on the grade-recovery curve, which typically means the maximization of recovery without going under a given concentrate grade limit. A more optimized control system would further move the operation of the circuit to a higher grade-recovery

curve (see Figure 2.2). The ultimate goal of the control, however, is to maximize the economic profit of the plant. The economic optimum is highly circuit dependent and varies also with time, as, for example, concentrate prices and operating costs change. In practice the grade and other property variations of the input ore constantly change the grade-recovery curve, and the goal of advanced control is to maximize the profit of the operation in spite of the disturbances (Laurila et al., 2002).

Even though automatic control systems are commonly used in concentration plants, fully automated mineral flotation processes capable of long-term unattended operation are scarce. This emphasizes the difficulty of flotation control, mainly caused by the complexity of the chemical and physical phenomena involved and by the variations of ore types, flotation response and throughput of the circuit. Consequently, the automatic control systems require human operators who monitor the operation and, if necessary, adjust the set points and alarm limits of the control system. The role of the operators is especially important in the cases of measurement equipment malfunction or during major disturbances like power failures.

2.2.2 Grade Measurements

Originally, mineral grade measurements of the process flows were performed by collecting samples and analyzing them visually by microscope or more accurately in the laboratory (Braden et al., 2002). However, process monitoring and control based on these methods was hindered by the subjectivity and difficulty of the visual inspection and by the delay of the laboratory analysis. On-line chemical analysis of the slurry streams was made possible by the development of the X-ray fluorescence (XRF) slurry analyzers in the early 1960s. On-stream analysis together with computers capable for process control calculations allowed the development of first on-line control systems.

The on-line XRF analyzers can be classified to two main types: on-stream and in-stream. The on-stream type consists of one centralized analyzer and requires separate sample lines that transfer the slurry from the sampling locations of the flotation circuit to the analyzer. The advantage of the centralized structure is that one analyzer probe can be used to provide assay information from many slurry lines. In addition, specially designed flow cells producing a controlled and reproducible turbulent slurry flow can easily be installed in the sample streams. This ensures good sample presentation, which is an essential prerequisite for a reliable slurry analysis by XRF. In in-stream analysis, on the other hand, each analyzer contains its own analyzer probe, which is typically installed directly in the measured process flow. Consequently, flow conditions may be inconsistent and the slurry samples are less representative. In most cases a centralized analyzer is also a more cost-effective solution for large flotation plants, where the number of slurry lines is high. (Cooper, 1976)

Recovery of the plant can be calculated if the volume and contents of the incoming ore and the final concentrate are known. A good indicator of decreased recovery is the increased concentration of the valuable minerals in the tailing flows. This typically implicates a disturbance in the process that leads to direct financial losses in the form of discarded valuable minerals. As a result, the tailing flows of the flotation plant

are carefully monitored by on-line analyzers. Obviously, the contents of the feed and final concentrate streams are also monitored to ensure that the requirements for the process efficiency and quality of the products are fulfilled. Additional assays in other process flows are used to monitor the proper operation of the individual flotation banks and to provide measurements that are used in the process control by human operators as well as by the automatic control system.

The economic effect of the on-line analysis in flotation plants has been investigated for example by Cooper (1976), and the importance of the analysis accuracy by Flintoff (1992). In addition to accuracy, Remes et al. (2007) studied the influence of analysis speed and sampling rate on the flotation control. They showed that the economic performance of a flotation process is significantly dependent on the sampling rate of the analysis, since faster sampling enables faster control actions as well. This result gives a good starting point for the work presented in this thesis.

2.3 The Pyhäsalmi Concentration Process

The measurements reported in this thesis were conducted at the Inmet Mining Corporation's Pyhäsalmi zinc, copper and sulfur mine located in Pyhäjärvi town in central Finland. The Pyhäsalmi ore contains mainly sulfides, namely pyrite, sphalerite and chalcopyrite. The main gangue minerals are barite and carbonates (see Table 2.1). In 2008 the annual production of the mine was about 1.4 million tonnes. The ore is currently mined underground between the 1050 m and 1416 m levels, and then crushed and hoisted to the surface for concentration. (Inmet Mining Corporation, 2009)

Table 2.1: The average composition of the ore concentrated at the Pyhäsalmi concentration plant. (Inmet Mining Corporation, 2008, 2009)

Mineral	Formula	Portion (%)	Usage	Notes
pyrite	FeS_2	65	sulfur	
sphalerite	$Zn_xFe_{1-x}S$	4	zinc	x = 0.95
chalcopyrite	$CuFeS_2$	3	copper	
pyrrhotite	$Fe_{1-y}S$	3	(gangue)	y = 0–0.17
barite	$BaSO_4$	-	(gangue)	
carbonates	$-CO_3$	-	(gangue)	

The concentration process at Pyhäsalmi contains three consecutive flotation circuits, one for separating each of the main products: copper (chalcopyrite), zinc (sphalerite) and sulfur (pyrite). The flotation is preceded by a semi-autogenous grinding stage, after which the particle size of the ore is about 65%—74 μm, meaning that 65% of the milled particle mass passes through a sieve with an aperture of 74 μm. (Inmet Mining Corporation, 2008)

The flowsheets of the copper and zinc flotation circuits are quite similar (Figure 2.3): They both consist of rougher, scavenger, middlings flotation and cleaner

flotation stages. The initial separation of the valuable minerals is performed in roughing, and the concentrates are pumped to cleaning. In scavenging, slowly floating particles of the rougher tailings are lifted to the middlings flotation banks to improve recovery, whereas the tailings are led to the final tailings of the circuit. The concentrate of the first middlings flotation cells is pumped to cleaning, whereas the rest of the concentrate is circulated back to the beginning of the stage. The copper circuit contains four cleaning stages and the zinc circuit three. The final tailings of the copper circuit are used to feed the zinc circuit, and the final tailings of the zinc circuit are further processed in the sulfur flotation circuit. Depending on the ore properties, a regrinding stage may be included in the zinc circuit to improve the recovery of sphalerite.

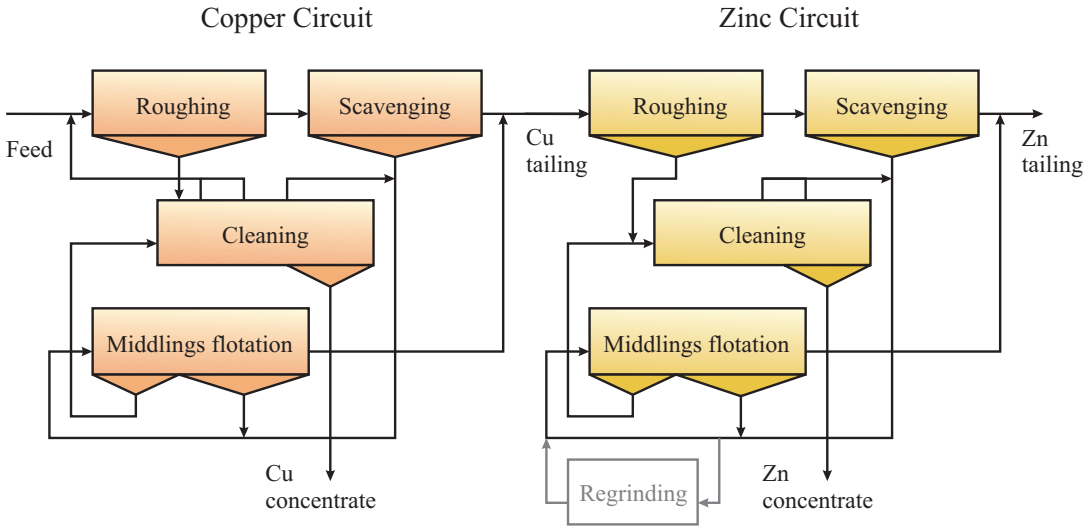

Figure 2.3: The general flowsheets of the copper and zinc flotation circuits at Pyhäsalmi.

The control of the Pyhäsalmi flotation process is highly automated. An essential part of the control is the centralized Outotec Courier® 6 SL on-stream XRF analyzer, which provides the elemental content measurements of the main slurry streams. Based on these, the automatic control system regulates, for example, the flotation reagent addition rates. (Wills and Napier-Munn, 2006)

Chapter 3

Reflectance Spectroscopy

Reflectance spectroscopy studies the light reflected, scattered or emitted from the target as a function of wavelength (Clark, 1999). The fundamental concept in reflectance spectroscopy is the interaction of incident light with the measured surface. Complex theories describing different special cases of the phenomenon exist, and a large number of applications especially in food, agricultural and pharmaceutical industry are based on the reflectance of light.

There are several reasons that make reflectance spectroscopy a tempting alternative, especially in the visible and near-infrared regions, for the more traditional methods (Hindle, 2008; Siesler, 2008): very little (if any) sample preparation is required; the measurement is fast; the instruments are relatively low-cost; no harmful radiation is used; contact with the investigated target is not necessary; the measurement is non-destructive. The main downside of reflectance spectroscopy is the large number of factors affecting the shape of the obtained spectra, which hinders the direct interpretation of the results.

This chapter provides a concise introduction to the basics of reflectance spectroscopy in order to provide some theoretical background for the reflectance spectral analysis conducted in this thesis. The main emphasis of the discussion is on diffuse reflectance spectroscopy, which takes place, for example, when light is scattered and reflected from particulated mineral samples. The general aspects of diffuse reflectance form the core of the discussion, but mineralogy specific theory and applications are presented as well. The approach in this chapter leans towards the more theoretical research conducted by the remote sensing community, whereas the next chapter reviews the importance of color measurements as an additional measurement in more practical mineral processing applications. Quite interestingly, the two starting points seem to converge into one in the very topic of this thesis.

3.1 Preliminaries

Spectroscopy can be performed in many wavelength ranges of the electromagnetic spectrum. The optical range, which covers the wavelengths between X-rays and radio

waves, is further investigated here. The International Electrotechnical Commission[1] defines the optical range from wavelengths around 1 nm to 1 mm and divides it into ultraviolet (UV, 1–400 nm), visible (VIS, defined as the range that causes a direct visual sensation, i.e. around 400–780 nm) and infrared (IR, optical wavelengths larger than the visible range) radiation. The infrared radiation can further be divided into near infrared (NIR), short-, mid-, and long-wavelength infrared (SWIR, MWIR, LWIR, respectively) and far-infrared radiation (FIR) (D'Amico et al., 2009). The NIR range is typically considered to cover the wavelengths starting from the end of the visible range (780 nm) and ending to 2500 nm (Ingle Jr. and Crouch, 1988). However, the terminology and the exact wavelength ranges are not standardized, and several variations exist (see e.g. Clark, 1999; D'Amico et al., 2009).

The research in this thesis utilizes the combined visible and near infrared (VNIR) reflectance spectroscopy. According to a common practice the VNIR range is considered to mean the wavelengths from 400 to 1000 nm, even though it is not a standard term (Clark, 1999). An advantage of the VNIR range is that the light can be detected by ordinary silicon-based sensors (D'Amico et al., 2009), which especially in the case of imaging spectroscopy means that low-cost CCD detectors can be used.

In reflectance spectral analysis the sample is typically stimulated with electromagnetic radiation, and the light intensity received from the sample is measured (Ingle Jr. and Crouch, 1988). If the incident light and reflected light have same angle with respect to the surface normal, the reflectance is said to be specular. Diffuse reflectance, on the other hand, takes place in powdered samples and matte surfaces, where the incident light is reflected to all directions from the surface because of scattering. When photons encounter granular material (e.g. grained mineral), they either reflect from the grain surfaces, pass through the grain or are absorbed. The photons that reflect from or refract through a particle may encounter other particles and finally be scattered away from the surface and reach the detector (Figure 3.1). Surfaces may also emit photons by themselves. In the following section, some of the main theoretical models used to describe diffuse reflectance are introduced.

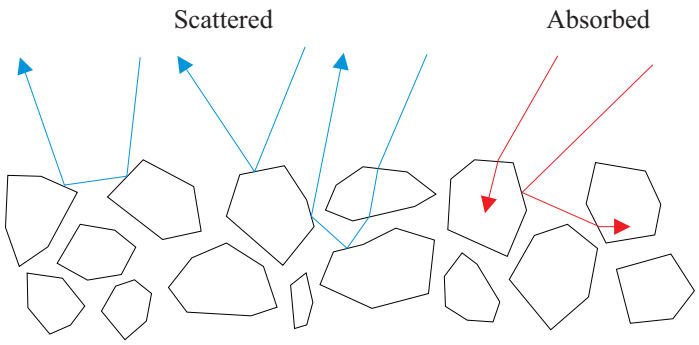

Figure 3.1: Scattering and absorption of light in a granular material.

[1] http://www.electropedia.org/

3.2 Diffuse Reflectance Models

The theoretical consideration of the reflectance phenomenon is a complex problem that does not have an unambiguous solution. The propagation of electromagnetic waves is described by the Maxwell equations (see e.g. Hapke, 2005). However, they cannot be solved in the general case that would cover all reflectance problems, and thus phenomenological laws with strict assumptions of the light and surface properties are more commonly used in practical applications.

This section presents two theories for light propagation and reflectance, mainly to be considered in selecting of a suitable preprocessing method for reflectance spectral data. The subject is more rigorously presented by Hapke (2005). For the following discussion, three quantities related to the interaction of light and a surface are introduced (Osborne et al., 1993): reflectance R, transmittance T and absorbance A. Reflectance of the surface is defined as the intensity ratio of the reflected I_{R} and indicent I_0 light:

$$R = \frac{I_{\mathrm{R}}}{I_0}. \tag{3.1}$$

Transmittance, on the other hand, describes the relative amount of intensity that passes through the sample:

$$T = \frac{I_{\mathrm{T}}}{I_0}, \tag{3.2}$$

where I_{T} is the transmitted intensity. Finally, absorbance is defined as

$$A = \log\left(\frac{I_0}{I_{\mathrm{T}}}\right) = \log\left(\frac{1}{T}\right). \tag{3.3}$$

3.2.1 Beer-Lambert Law

The absorption of light traveling in a homogenenous and non-scattering medium is described by the Beer-Lambert law, which states that the intensity I of the light is exponentially decreasing with respect to the distance b:

$$I = I_0 e^{-kb}, \tag{3.4}$$

where I_0 is the original intensity of the light and k the linear absorption coefficient (Griffiths and Dahm, 2008). The absorption coefficient is assumed to be linearly dependent on the concentration of the absorbent ($k = ac$), and thus a linear relationship between the concentration c and absorbance A of a sample with the thickness b can be derived:

$$A = \log\left(\frac{I_0}{I_{\mathrm{T}}}\right) = acb, \tag{3.5}$$

where a is the molar absorptivity of the absorber (Osborne et al., 1993).

In practice, there are several factors that violate the assumptions of the Beer-Lambert law (Osborne et al., 1993). Scattering, for example, should not be neglected especially in granular materials.

In the case of reflectance of light from a surface of a thick sample, absorbance of the surface is calculated as:

$$A = \log\left(\frac{I_0}{I_\mathrm{R}}\right) = \log\left(\frac{1}{R}\right). \tag{3.6}$$

This can be combined with (3.5) to obtain a linear relationship between the $\log(1/R)$ transformed reflectance and absorbent concentration c (Workman Jr., 2008):

$$\log\left(\frac{1}{R}\right) \propto c. \tag{3.7}$$

3.2.2 Kubelka-Munk

The Kubelka-Munk (K-M) theory describes the interaction of light and a surface using two light fluxes in opposite directions. The material is characterized by the absorption coefficient k and the scattering coefficient s. Assumptions of the K-M theory are that the surface of the sample is infinitely large (no edge effects), the light scattering particles are evenly distributed, particle dimensions are small with respect to the sample thickness and that the whole sample is homogeneously illuminated with a monochromatic diffuse light source (Ciani et al., 2005).

In the special case of diffuse reflectance (the sample thickness is assumed infinitely large), the K-M theory reduces into a simple form:

$$\frac{k}{s} = \frac{(1-R)^2}{2R} \equiv f(R), \tag{3.8}$$

where $f(R)$ is the K-M function (Osborne et al., 1993). Since $k = ac$, the relation between the reflectance and concentration can be written as:

$$f(R) = \frac{ac}{s}, \tag{3.9}$$

indicating that the K-M function is linearly proportional to the concentration of the absorbing substance in the sample.

3.3 Reflectance Spectroscopy in Mineralogy

Optical reflectance spectroscopy of minerals is based on the distinctive absorption properties of the different mineral species. In the following, the theory of absorption in minerals is briefly introduced, and some mineralogy-related applications of spectroscopy are presented.

3.3.1 Theory

The key concept in optical reflectance spectral analysis of minerals is absorption, and there are several wavelength dependent absorption mechanisms. The two main causes for absorption are electronic and vibrational processes. Clark (1999) provides

a concise review of the subject, and a more detailed discussion is given by Burns (1993). The following review is based on these two publications.

Electronic absorption occurs when the incident photon is absorbed by a molecule in the sample, and one or more electrons are moved to higher energy levels. When the electrons return back to the lower energy levels, they emit photons. However, the emitted photons do not typically have the same wavelength as the incident photons, meaning that the incident wavelength is absorbed. Several electronic processes cause absorption in mineral structures: crystal field transitions, electron transfer between transition metal ions, and charge transfer between transition metal ions and anions. The lattice structure and electrons shared with several atoms increase the possible absorption energies, resulting in diverse spectral features of minerals.

Vibrational absorption is related to the vibration of the molecule: the chemical bonds between the atoms act like springs connecting mass points (the atoms), and the energy of the absorbed photon causes the whole molecule to vibrate. Each molecule has a set of fundamental vibration modes that correspond to the possible absorption frequencies. The vibrational absorbance in minerals is characterized by the vibrational modes of the mineral structure. Depending on the molecular structure, different vibrations are possible. The frequencies of the fundamental modes typically reside in the MWIR region, but overtones and combinations of them may affect also the higher frequency regions like visible and near-infrared. Especially carbonates and minerals with water or hydroxyl groups are prone to vibrational absorption.

The particle size of the mineral sample has an effect on the absorption properties as well. If the reflectance phenomenon is dominated by multiple scattering, the intensity of the reflected light decreases as the particle size increases. However, depending on the wavelength range and the type of mineral, also the opposite can be true as demonstrated in Section 6.1.

3.3.2 Applications

A traditional and broad application area of reflectance spectroscopy is remote sensing (see e.g. Campbell, 2006; Rencz, 1999), where the light reflected from Earth's or planetary surfaces is studied. The measurements are performed from aircraft or satellites, or by telescopes in the case of planetary targets. While the spectra can be used to analyze different aspects of the surface (vegetation, hydrology, agriculture), the mineralogy-related information obtained can be used, for example, to produce mineral maps (Hook et al., 1999) or to study the geology of planets (Bell III et al., 1999). A personal discussion about the history of hyperspectral remote sensing of Earth provided by Goetz (2009) indicates that the main motivation in the field has been the mineralogical mapping of soils and outcrops. For example, the remote sensing of ophiolites (regions of Earth's oceanic crust that have been lifted to the surface) has been intensively investigated (Khan and Mahmood, 2008).

In astronomical studies remote sensing is often the only way to analyze the composition of planets, satellites, asteroids and other astronomical surfaces. Bell III et al. (1999) review the topic and emphasize the importance of optical reflectance spectroscopy in measuring the mineralogy of planetary surfaces. The studied wave-

length range is typically from 300 to 3500 nm, where the intensity of the sunlight is the largest. Recent studies on the subject have been published, for example, by Fornasier et al. (2008) and Cloutis et al. (2008).

The application of reflectance spectroscopy to ore analysis in mineral exploration and mineral engineering is discussed in detail in the next chapter.

Chapter 4

Color and Spectral Measurements in Mineral Engineering

Monitoring of flotation processes in many flotation plants is partially based on the visual inspection of the froth appearance and color by the human operators. It is a generally accepted fact that especially the color of froth in some mineral flotation processes correlates with the mineral contents (Bartolacci et al., 2006; Gebhardt et al., 1993; Hätönen, 1999; Liu et al., 2005). This has motivated the utilization of machine vision for analyzing the froth properties to gain additional information on the state of the process. Machine vision has also been applied to automatic detection and mineral quantification of rock samples and ore transported on belt conveyors. Reflectance spectroscopy is further used in more recent studies especially as a rapid method to analyze mineral exploration drill cores.

This chapter reviews the importance of color measurements in practical mineral processing applications, starting from the earlier studies utilizing regular video cameras and ending in the latest research with advanced spectrographs. At the same time, the versatility of analysis methods in mineral engineering based on the properties of reflected light is demonstrated. The applications summarized in this chapter form the starting point for the research conducted in the thesis.

4.1 Froth Image Analysis

The most common application of machine vision in mineral flotation is the froth image analysis. In these studies, cameras are installed on top of the flotation cells and the froth structure is extracted from the froth images. Segmentation of the images has been an important image processing step already from the first studies (Symonds and De Jager, 1992), followed by the extraction of froth features like bubble size, bubble shape, mineral load on bubbles, etc. (Bonifazi et al., 1998; Cipriano et al., 1998; Kaartinen et al., 2006b; Sadr-Kazemi and Cilliers, 1997). Algorithms for froth speed and bubble collapse rate have also been presented and correlations of these variables with froth grades have been calculated (Cipriano et al., 1998; Holtham and Nguyen, 2002; Kaartinen et al., 2006b).

Another popular approach for analyzing the images is to calculate the features as statistical properties of the image data. For example, the (fast) fourier transform (FFT) (Moolman et al., 1994), gray level dependence matrix (Moolman et al., 1995) or multivariate image analysis (MIA) (Bartolacci et al., 2006; Liu et al., 2005) methods can be used.

Usually the initial aim of the froth image analysis is to classify the state of the froth phase and to evaluate how well the process is performing. This information can be used to assist the process operators, especially the less experienced ones, when deciding the required control actions. Ultimately the goal of these studies is to utilize the visually measured features in automatic feedback control.

4.1.1 The Importance of Color

Whereas the segmentation-based algorithms clearly do not fully utilize the image color information, some of the statistical methods do, at least indirectly. Liu et al. (2005) actually state that the morphological properties of the froth are not highly correlated with the color information, which they further assume to mainly describe the froth mineral contents. As a consequence, they separately analyze the color information and morphology of the froth images by an advanced MIA algorithm combined with wavelet analysis and PCA in order to describe how healthy the froth is. The results are utilized in a simulated feedback control scheme in the following work (Liu and MacGregor, 2008) with promising results.

In addition to the image analysis, pure color measurements of the froths and slurries have been analyzed as well. Earlier studies only consider the intensity of the light reflected from the froth. For example, Moolman et al. (1994) show that in a copper flotation bank the intensity histogram can be used to quantify the froth copper grade. However, later the color information in the images is extracted in the full red, green and blue (RGB) color space and typically used as a part of the features in the image analysis process (Cipriano et al., 1998; Morar et al., 2005).

Kaartinen et al. (2006b) use an RGB camera-based machine vision system in a zinc flotation circuit to measure different morphological and color features of the froth in the rougher stage at the Pyhäsalmi concentration plant. They demonstrate the general correlations between the image variables and process measurements during a long period of normal operation. Especially the red color of the froth is shown to correlate with the final zinc grade as well as with the other properties of the froth. The camera measurements—among them the red color value—are further utilized in an automatic expert controller for regulating the addition of the activator chemical (copper sulfate). It is shown that the process performance and thus also the profitability of the plant were significantly improved after the implementation of the controller.

4.1.2 Commercial Products

The research efforts briefly summed above have led to a few commercial froth image analyzer products: ACEFLOT (Cipriano et al., 1998), JKFrothCam (Holtham

and Nguyen, 2002), SmartFroth (Morar et al., 2005), Outotec's Frothmaster^{TM} and Metso Minerals' VisioFroth. The overall structure and operation principle of all these products is quite similar, since in every one of them an RGB camera is mounted on top of a flotation cell and the captured images are processed on a computer to extract both the morphological froth features as well as the color of the froth.

4.2 Froth and Slurry Assaying Based on Color

The most interesting studies regarding the topic of this thesis are the ones where pure color measurements are utilized for assaying purposes in flotation plants. When focusing only on the color of the minerals, the analysis can be extended from flotation froths to mineral slurries and dry mineral measurements. Among the first publications in this area are the works by Gebhardt et al. (1993) and Oestreich et al. (1995). As with the image analysis approach, these early studies have limitations related to the color measurement devices. Gebhardt et al. (1993) use a sensor that can measure color as an adjustable linear combination of the red, green and amber reflectance values. This scalar is correlated with the mineral contents of dry pure mineral and mineral mixture samples as well as with mineral-loaded flotation froths both in laboratory and in plant conditions. The studied minerals are quartz, pyrite, chalcopyrite and molybdenite. The results show quite strong and surprisingly linear relations between the measured color values and the weight ratios in the sample mineral mixtures. A linear relation was found as well between the froth color signal and the chalcopyrite-pyrite and chalcopyrite-molybdenite ratios in real plant tests, whereas the molybdenite-chalcopyrite ratio was reflected nonlinearly in the color value. In general, however, it was shown that the color measurements can readily reveal at least the larger changes in mineral contents of the dry mineral mixtures and froths in case of these minerals.

Oestreich et al. (1995) continued the research by utilizing RGB video cameras in the analysis of chalcopyrite-molybdenite mixtures. One important addition introduced in the study was the usage of color vector angle, a scalar measure of the ratio of two pre-defined colors, "chrominance red" and "chrominance blue", present in the measured color. The color vector angle was shown to be less affected by the changes in lighting and shadow variations as well as to correlate better with the mineral contents than the original RGB values. Another addition was to extend the analysis to mineral slurries, whose color was also shown to correlate with the mixture ratio. However, only artificial mixture samples were measured and the variation range in the chalcopyrite-molybdenite ratio was as large as from 0 to 100 percent.

Color analysis has been investigated also in coal flotation as a method to estimate the contents of the froth. There the interest is especially in the ash content, and for example Hargrave et al. (1996) have shown that correlations exist between the gray level distribution and ash content of coal flotation froth. Color analysis has been extended to tin flotation as well, for example by Hargrave and Hall (1997), who showed that the relative redness value of the flotation froth can be used to estimate the grade.

If only the color is measured, a spectrometer can be used instead of an RGB camera to obtain more accurate color information. Surprisingly, very few studies are published on the application of spectroscopy in the analysis of mineral flotation froths or slurries. One preliminary attempt to measure and analyze the visible range spectrum of zinc flotation froths was presented by Kaartinen (2001). However, because of problems with measurement arrangements and dirty conditions, only a small amount of data was gathered which prevented a proper analysis. Another spectrum based approach initially concentrating on dry mineral mixtures has been introduced and commercialized by Blue Cube Systems, as discussed in the following section.

4.2.1 Commercial Products

Even though the color analysis in mineral flotation grade estimation has given promising results in scientific studies, only few actual products utilizing the concept are on the market. South African based Blue Cube Systems[1] manufactures a set of products for on-line measuring the grades of dry, slurry or filter cake form mineral mixtures. The technology is based on diffuse reflectance and transmission spectroscopy apparently in the visible and near-infrared wavelength range. A set of representative calibration samples is required to form the so-called fingerprints of the different minerals present in the mixtures. However, no proper scientific publications explaining the technical details of the modeling methods or spectral measurements are available.

Initially the system was applied to dry mineral mixtures (Reyneke et al., 2003), where the spectra of dry samples of rutile and zircon rich mineral mixtures were measured in laboratory conditions and compared with grain counting results. Relatively good estimation results were obtained for validation data, and especially the main mineral grades were predicted with a good accuracy. De Waal and Du Plessis (2005) demonstrated the method in the on-line measurement and control of a high tension roll separator test circuit, mainly to emphasize the possibilities of automatic control. Additionally, De Waal (2007) discussed the technology and some available products at a very general level. A case-study application of the The BlueCube MQi slurry analyzer to platinum slurry is described in (Blue Cube Systems Ltd, 2009). For a small number of samples, good precision and accuracy is obtained in measuring the chromite and platinum group metal contents of the slurry.

Based on the reviewed literature, the Blue Cube technology requires an initial calibration with known mineral mixtures, after which the mineral composition measurements can be conducted on-line and in-stream at real concentration plants. The analysis results are directly available and the sampling interval is short. However, no proper studies of the long term accuracy of the product are published.

[1] `http://www.bluecubesystems.com`

4.3 Other Color Measurements

Other applications of the color measurements are commonly utilized in mineral engineering as well. Mainly the purpose is to determine the contents of ores either in mineral exploration or during the concentration process.

4.3.1 Rocks on Conveyors

An initial color-based analysis on mineralogy and lithology of rocks in mineral engineering was published by Marschallinger (1997), who used the color information to automatically classify rocks in RGB images. The purpose was to provide a faster and less tedious way to quantify the amount and spatial distribution of different minerals in rock samples. Casali et al. (2001) applied the RGB image analysis of rocks on a conveyor belt feeding a grinding circuit to determine the ore work index for grindability estimation. Several rock-specific features including color were calculated from RGB images, and a neural network was used to obtain the lithological composition of the rocks with a good precision. This information was further utilized in estimating the operating work index and in evaluating the efficiency of the grinding circuit. A corresponding study reported by Tessier et al. (2007) analyzed the more challenging nickel mineral system with both dry and wet samples.

Reflectance spectroscopy has been only recently utilized for ore analysis on conveyor belts. The study by Goetz et al. (2009) introduced a measurement setup where visible and NIR (350–2500 nm) reflectance spectroscopy is applied to determine the amount of gangue minerals in copper ore samples and the oxide contents of limestone. The measurement uses a PLS calibration model with X-ray diffraction (XRD), XRF and cation exchange capacity (CEC) analyses as the reference data. Good validation results are obtained for the laboratory measurements (R^2 ranging from 0.66 to 0.9), suggesting that the method could be used in real process conditions as well. Another laboratory study describing the usage of VNIR reflectance spectroscopy for detecting gangue from zinc and copper ore is reported by Pietilä and Haavisto (2009). They emphasize the importance of correct preprocessing and apply a PLS-based discriminant analysis (PLS-DA) to classify the samples with a good precision.

At least three commercial spectral measurement systems suitable for rock classification on conveyor belts are available: VisioRock (Metso Minerals) (Guyot et al., 2004), the QS series (ASD) used by Goetz et al. (2009) and Solbas (ABB). The first one, VisioRock, utilizes RGB cameras and is mainly used to determine the particle size of the rocks, whereas the latter two are based on the combined visible and NIR reflectance spectroscopy.

4.3.2 Drill Cores and Mineral Exploration

Core drilling is a mineral exploration method used to determine the abundance of minerals in possible deposits and to spatially map the location of the ore. The core samples are traditionally analyzed in laboratory by, for example, XRD. The analysis involves extensive sample preparation with splitting, crushing and drying of

the core pieces. Kruse (1996) suggested the usage of NIR reflectance spectroscopy as an alternative method for split core analysis. The study showed that it is possible to produce mineralogical maps of drill cores based on the reflectance spectra. The detected minerals were kaolinite, illite, montmorillonite and chlorite, the first three of which have strong absorption bands in the NIR region.

Taylor (2000) further analyzed the ground drill core samples with visible and NIR (350–2500 nm) reflectance spectroscopy, and compared the results to XRD analysis. The main minerals were muscovite, illite, pyrite, quartz and carbonates. Even though quite weak correlations between the reflectance spectrum and XRD analysis results were obtained, the study concluded that the reflectance spectroscopy is a quick and cost-effective method to analyze the drill cores.

In mineral exploration, reflectance spectroscopy of drill cores and surface samples is utilized, for example, by Squire et al. (2007), who study the spatial mineral distribution of an Au-Cu deposit. An analogous study is reported by Yang et al. (2005). Commercial drill core analyzers based on reflectance spectroscopy are available as well (see e.g. Mauger and Huntington, 2005), and several portable spectrometer systems for more general measurement purposes can be found.

Chapter 5

Data-Based Multivariate Methods

Linear multivariate regression methods are a common choice for data-based analysis of spectral measurements. Chemometrics (see e.g. Gemperline, 2006) studies the utilization of mathematics and statistics to data obtained from chemical systems, and the interpretation of high-dimensional spectral measurements with linear multivariate methods is one of the most typical applications in the field. In all the related publications, multivariate regression is extensively applied to the analysis of the measured VNIR reflectance spectral data of the flotation froths and slurries. In addition, the plant-wide oscillations in the copper circuit are analyzed in Publication **VI** with a recursive version of singular spectrum analysis (SSA), which is strongly related to principal component analysis (PCA).

This chapter reviews the most common multivariate regression methods and discusses the data preprocessing and evaluation of results. The emphasis of the chapter is on the importance of the data covariance structures. Basically all the presented regression models can be calculated from the covariances, even if the original data are unknown. This property is further utilized when adaptive or recursive calculation of the regression models is discussed. Data preprocessing as well as regression model evaluation and validation are briefly summarized, and SSA is introduced in order to provide the reader with sufficient knowledge for the rest of the study.

5.1 About Data

Consider a set of n random variables $\{X_1, X_2, \ldots, X_n\}$ that is distributed according to the multivariate probability distribution function $f(x_1, x_2, \ldots, x_n)$. The mean and variance of each random variable are denoted as μ_{X_i} and $\sigma^2_{X_i}$, respectively. The mean values of the variables can be collected as the elements of the mean vector

$$\boldsymbol{\mu}_x = \begin{bmatrix} \mu_{X_1} & \mu_{X_2} & \cdots & \mu_{X_n} \end{bmatrix}^T. \tag{5.1}$$

The covariance of two random variables is defined as

$$r_{X_i X_j} = E\left[(X_i - \mu_{X_i})\left(X_j - \mu_{X_j}\right)\right], \tag{5.2}$$

and the covariance matrix of the multivariate distribution is

$$\boldsymbol{R}_x = \begin{bmatrix} r_{X_1X_1} & r_{X_1X_2} & \cdots & r_{X_1X_n} \\ r_{X_2X_1} & r_{X_2X_2} & \cdots & r_{X_2X_n} \\ \vdots & & \ddots & \vdots \\ r_{X_nX_1} & r_{X_nX_2} & \cdots & r_{X_nX_n} \end{bmatrix}. \tag{5.3}$$

The covariance matrix (5.3) describes the linear correlation structure of the set of random variables: The diagonal elements of $\boldsymbol{R}_x$ are the variances of the individual variables, and the non-diagonal elements contain the covariances between all possible random variable pairs in the set.

Typically in practical modeling problems, only a finite number of samples of the random variables is available, whereas the data distributions are unknown. Thus the multivariate probability distribution parameters (5.1) and (5.3) have to be estimated from the data. Assuming that $\boldsymbol{x} = [x_1\, x_2 \cdots x_n]^T$ represents one sample of the random variables $\{X_1, X_2, \ldots, X_n\}$, and a data set of N samples is collected as the rows of the data matrix

$$\boldsymbol{X} = \begin{bmatrix} \boldsymbol{x}(1) & \boldsymbol{x}(2) & \cdots & \boldsymbol{x}(N) \end{bmatrix}^T, \tag{5.4}$$

the sample mean is calculated as

$$\hat{\boldsymbol{\mu}}_x = \begin{bmatrix} \hat{\mu}_{X_1} & \hat{\mu}_{X_2} & \cdots & \hat{\mu}_{X_n} \end{bmatrix}^T = \frac{1}{N}\sum_{k=1}^{N} \boldsymbol{x}(k). \tag{5.5}$$

If normal distribution is assumed and the samples are independent, then (5.5) is the maximum likelihood estimate of $\boldsymbol{\mu}_x$ (Anderson, 2003).

The covariance structure of the probability distribution can also be estimated from the data. Depending on the scaling and centering of the data in $\boldsymbol{X}$, different measures of the association between the variables can be defined. According to Basilevsky (1994), the general term for the group of matrices describing the covariance structure is association matrix. The possible types of association matrices with non-centered data are inner product matrix (original data) or cosine matrix (data scaled to unit variance). However, other kinds of nomenclature also exist (Carroll et al., 1997). If mean-centered data are used, the possible association matrices are covariance matrix (data mean-centered) and correlation matrix (data scaled to unit variance and mean-centered) (Basilevsky, 1994; Carroll et al., 1997; Jackson, 2003). The data origin as well as units and scaling of the individual variables affect whether the covariance or correlation matrices should be used as the starting point of multivariate analysis (Jackson, 2003).

In the rest of this work, the data vectors in $\boldsymbol{X}$ are assumed to be appropriately preprocessed (as further discussed in Section 5.4), and the general term sample covariance matrix (or just covariance matrix) is used for the estimate

$$\hat{\boldsymbol{R}}_x = \frac{1}{N}\boldsymbol{X}^T\boldsymbol{X}. \tag{5.6}$$

In the case of normally distributed variables and assuming that the data are independent and mean-centered, (5.6) is the maximum likelihood estimate of $\boldsymbol{R}_x$ (Anderson, 2003). The normalization directly by the number of samples N in (5.6) leads to a biased estimate of the real covariance, if also the subtracted mean is estimated from the data (Anderson, 2003). However, if the data set is large, the bias can be assumed negligible.

The sample cross-covariance between two multivariate datasets, $\boldsymbol{X}$ and $\boldsymbol{Y}$, is further measured by the cross-covariance matrix

$$\hat{\boldsymbol{R}}_{xy} = \frac{1}{N}\boldsymbol{X}^T\boldsymbol{Y}. \tag{5.7}$$

The elements of (5.7) represent the sample covariances between the individual components of $\boldsymbol{x}$ and $\boldsymbol{y}$.

5.2 Multivariate Regression Methods

The aim in multivariate regression is to find a linear mapping $\boldsymbol{B}$ between the n-dimensional predictor vector $\boldsymbol{x}$ and the m-dimensional response vector $\boldsymbol{y}$:

$$\boldsymbol{y} = \boldsymbol{B}\boldsymbol{x} + \boldsymbol{e}, \tag{5.8}$$

where $\boldsymbol{e}$ is the modeling error. The mapping is estimated using N samples collected from both predictor and response variables, and stored in the matrix $\boldsymbol{B}$. Assuming that the predictor data are collected in the N rows of matrix $\boldsymbol{X}$ and the response data in the N rows of matrix $\boldsymbol{Y}$, the full matrix equation is

$$\boldsymbol{Y} = \boldsymbol{X}\boldsymbol{B}^T + \boldsymbol{E}, \tag{5.9}$$

where $\boldsymbol{E} = [\boldsymbol{e}(1)\,\boldsymbol{e}(2)\,\cdots\,\boldsymbol{e}(N)]^T$ contains the error vectors for each predictor and response sample pair.

The common property of the multivariate regression models presented in the following is that they estimate such model matrix $\boldsymbol{B}$ that keeps the modeling error $\boldsymbol{E}$ small in some sense. An existing model matrix can be used to predict the response for a new predictor sample:

$$\hat{\boldsymbol{y}} = \boldsymbol{B}\boldsymbol{x}. \tag{5.10}$$

5.2.1 Multivariate Least Squares

The least squares (LS) solution for the multivariate regression model estimation is simply to minimize the sum of squared modeling errors for each response variable:

$$\boldsymbol{b}_{\mathrm{LS},i} = \arg\min_{\boldsymbol{b}^*_{\mathrm{LS},i}} \left\{ \left(\boldsymbol{y}_i - \boldsymbol{X}\boldsymbol{b}^*_{\mathrm{LS},i}\right)^T \left(\boldsymbol{y}_i - \boldsymbol{X}\boldsymbol{b}^*_{\mathrm{LS},i}\right) \right\} = \arg\min_{\boldsymbol{b}^*_{\mathrm{LS},i}} \{\boldsymbol{e}_i^T\boldsymbol{e}_i\}, \tag{5.11}$$

where $\boldsymbol{b}_{\mathrm{LS},i}$ is the i:th column of the LS model matrix $\boldsymbol{B}_{\mathrm{LS}} = [\boldsymbol{b}_{\mathrm{LS},1}\,\boldsymbol{b}_{\mathrm{LS},2}\,\cdots\,\boldsymbol{b}_{\mathrm{LS},m}]$. The vectors $\boldsymbol{y}_i$ and $\boldsymbol{e}_i$ are the i:th columns of $\boldsymbol{Y}$ and $\boldsymbol{E}$, respectively.

The LS model matrix can be easily calculated using the pseudoinverse of $\boldsymbol{X}$ (Martens and Næs, 1989):

$$\boldsymbol{B}_{\mathrm{LS}} = \left(\boldsymbol{X}^T\boldsymbol{X}\right)^{-1}\boldsymbol{X}^T\boldsymbol{Y} = \boldsymbol{X}^{+}\boldsymbol{Y}. \tag{5.12}$$

Essentially, (5.12) is formed by the inverse of the predictor covariance matrix and the cross-covariance matrix of the predictors and reponses:

$$\boldsymbol{B}_{\mathrm{LS}} = \hat{\boldsymbol{R}}_x^{-1}\hat{\boldsymbol{R}}_{xy}. \tag{5.13}$$

If two or more variables in $\boldsymbol{X}$ are linearly dependent, the inverse $\hat{\boldsymbol{R}}_x^{-1}$ does not exist, and the LS estimate cannot be calculated. This kind of collinearity commonly appears in spectroscopy because of smooth spectral curves. When noisy data are utilized in practice, the variables can typically be only almost collinear, which leads to numerical problems in the inversion of the covariance matrix. As a result, the LS estimate obtained may not be accurate nor stable (Martens and Næs, 1989). One of the simplest strategies (Basilevsky, 1994) to deal with the collinearity is ridge regression, where a small positive quantity is artificially added to each diagonal element of the predictor sample covariance matrix (Hoerl and Kennard, 1970). However, ridge regression does not take into account the structure of the data, and is therefore considered merely as a technical trick to make the covariance matrix invertible (Basilevsky, 1994; Hyötyniemi, 2001).

5.2.2 Principal Component Regression

Principal component regression (PCR) (Basilevsky, 1994; Martens and Næs, 1989) handles the collinearity issue by first performing principal component analysis (PCA) (Basilevsky, 1994; Wold et al., 1987) of the predictor data and then connecting the PCA scores to the response variables using multivariate LS estimation. In PCA, the data matrix $\boldsymbol{X}$ of rank d is decomposed into a sum of d outer products of score and loading vectors:

$$\boldsymbol{X} = \boldsymbol{t}_1\boldsymbol{p}_1^T + \boldsymbol{t}_2\boldsymbol{p}_2^T + \cdots + \boldsymbol{t}_d\boldsymbol{p}_d^T = \boldsymbol{T}\boldsymbol{P}^T \tag{5.14}$$

The loading vectors or principal component directions $\boldsymbol{P} = [\boldsymbol{p}_1\, \boldsymbol{p}_2\, \cdots\, \boldsymbol{p}_d]$ can be interpreted as unit vectors indicating the orthogonal directions of maximum variance in $\boldsymbol{X}$. Accordingly, the score vectors in $\boldsymbol{T} = [\boldsymbol{t}_1\, \boldsymbol{t}_2\, \cdots\, \boldsymbol{t}_d]$ give the weighting coefficients of the loadings for each data point in $\boldsymbol{X}$. The importance of each principal component (PC) is measured by the variance λ_i of the corresponding score vector $\boldsymbol{t}_i$. Normally the PCs are ordered according to the variance they capture, that is, $\lambda_1 \geq \lambda_2 \geq \ldots \geq \lambda_d$.

There are two main approaches for calculating PCA: the nonlinear iterative partial least squares (NIPALS) algorithm that operates on the original data matrix $\boldsymbol{X}$, and the eigenvalue decomposition of the data covariance matrix $\hat{\boldsymbol{R}}_x$. The NIPALS algorithm was originally developed by Wold (1966), and is commonly utilized also in PLS calculation. It has been shown that the NIPALS solution is equal to the one obtained by the eigenvalue method (Geladi and Kowalski, 1986).

The eigenvalue method is based on the fact that the eigenvalue decomposition of the data covariance gives the PCA loadings as eigenvectors:

$$\hat{\boldsymbol{R}}_x = \boldsymbol{P}\boldsymbol{\Lambda}\boldsymbol{P}^T, \tag{5.15}$$

and the eigenvalues on the diagonal of $\boldsymbol{\Lambda} = \mathrm{diag}\{\lambda_1, \lambda_2, \ldots, \lambda_d\}$ indicate the variance captured by each PC. Thus the PCA loadings can be determined without utilizing the actual data matrix $\boldsymbol{X}$. Given the data, the score vectors are further obtained as

$$\boldsymbol{T} = \boldsymbol{X}\boldsymbol{P}. \tag{5.16}$$

The advantage of PCA is that it effectively captures the structural collinearities in the predictor variables. It can be assumed that the first PCs contain the relevant data structure, whereas the last ones can be interpreted as noise. The dimension of the original data can thus be efficiently reduced by using only the $l < d$ main PCs to approximate $\boldsymbol{X}$:

$$\boldsymbol{X} \approx \boldsymbol{t}_1\boldsymbol{p}_1^T + \boldsymbol{t}_2\boldsymbol{p}_2^T + \cdots + \boldsymbol{t}_l\boldsymbol{p}_l^T = \boldsymbol{T}_l\boldsymbol{P}_l^T \tag{5.17}$$

The space spanned by the selected loadings $\boldsymbol{P}_l = [\boldsymbol{p}_1\, \boldsymbol{p}_2\, \cdots\, \boldsymbol{p}_l]$ is the PCA subspace.

PCR utilizes the orthogonality of the scores when calculating the regression; instead of using the original predictors, the selected main score variables are utilized in the LS mapping:

$$\boldsymbol{Y} = \boldsymbol{T}_l\tilde{\boldsymbol{B}}_{\mathrm{PCR}}^T + \boldsymbol{E}, \quad \text{where} \quad \tilde{\boldsymbol{B}}_{\mathrm{PCR}} = \left(\boldsymbol{T}_l^T\boldsymbol{T}_l\right)^{-1}\boldsymbol{T}_l^T\boldsymbol{Y}. \tag{5.18}$$

The PCR estimate for the mapping $\boldsymbol{B}$ in (5.9) is obtained by combining (5.18) with (5.16):

$$\boldsymbol{B}_{\mathrm{PCR}} = \boldsymbol{P}_l\tilde{\boldsymbol{B}}_{\mathrm{PCR}} = \boldsymbol{P}_l\left(\boldsymbol{T}_l^T\boldsymbol{T}_l\right)^{-1}\boldsymbol{T}_l^T\boldsymbol{Y} = \boldsymbol{P}_l\left(\boldsymbol{P}_l^T\boldsymbol{X}^T\boldsymbol{X}\boldsymbol{P}_l\right)^{-1}\boldsymbol{P}_l^T\boldsymbol{X}^T\boldsymbol{Y} \tag{5.19}$$

Again, the mapping can be written using the covariances $\hat{\boldsymbol{R}}_x$ and $\hat{\boldsymbol{R}}_{xy}$ instead of the data matrices:

$$\boldsymbol{B}_{\mathrm{PCR}} = \boldsymbol{P}_l\left(\boldsymbol{P}_l^T\hat{\boldsymbol{R}}_x\boldsymbol{P}_l\right)^{-1}\boldsymbol{P}_l^T\hat{\boldsymbol{R}}_{xy}. \tag{5.20}$$

Since the loadings are obtained using (5.15), only the covariances $\hat{\boldsymbol{R}}_x$ and $\hat{\boldsymbol{R}}_{xy}$ are required to calculate the PCR model.

The advantage of PCR over LS solution is that the collinearity problem is effectively avoided by PCA. Because only the main principal components with eigenvalues larger than zero are utilized in the LS model included in PCR, the score covariance matrix is always invertible. Moreover, the PCA results can be used to analyze the structure of the predictor data, which may increase the interpretability of the model. The downside of PCR is that it is more complex to calculate, and some relevant information may be lost by the omitted principal components (Geladi and Kowalski, 1986). Additionally, the latent variables in PCR are determined from the predictor data only, even though also the response data should be considered.

5.2.3 Partial Least Squares

Partial least squares (PLS) (Geladi and Kowalski, 1986; Martens and Næs, 1989; Wold et al., 2001) is the main multivariate regression method used in Publications **I**–**V** and **VII**, and is thus more thoroughly discussed here. PLS was originally introduced by Wold (1965) and improved by Wold et al. (1983), and has since then become a standard method in chemical applications (Bjørsvik and Martens, 2008; Gemperline, 2006). In comparison to PCR where only the predictor data structure is taken into account, PLS models the structure of both the predictor and response data. This may improve the regression model performance in situations where the predictor contains a large variance component which is not related to the changes in the responses. However, the calculation process of PLS is more complicated than that of PCR.

In PLS, a set of l latent variables is used to approximate the predictor data:

$$\boldsymbol{X} = \boldsymbol{T}\boldsymbol{P}^T + \boldsymbol{F}, \tag{5.21}$$

where the $N \times l$ matrix $\boldsymbol{T}$ contains the PLS scores of the predictors, and $\boldsymbol{P}$ $(n \times l)$ the corresponding PLS loadings. The residuals are collected in $\boldsymbol{F}$. The orthogonal predictor scores $\boldsymbol{T}$ are related to the predictor data by predictor weights in the $n \times l$ matrix $\boldsymbol{W}^*$:

$$\boldsymbol{T} = \boldsymbol{X}\boldsymbol{W}^*. \tag{5.22}$$

It is further assumed that the predictor scores can be used to explain the response data as well:

$$\boldsymbol{Y} = \boldsymbol{T}\boldsymbol{C}^T + \boldsymbol{E} = \boldsymbol{X}\boldsymbol{W}^*\boldsymbol{C}^T + \boldsymbol{E} = \boldsymbol{X}\boldsymbol{B}_{\mathrm{PLS}} + \boldsymbol{E}, \tag{5.23}$$

where $\boldsymbol{C}$ contains the response weights, $\boldsymbol{B}_{\mathrm{PLS}}$ is the final PLS mapping matrix, and the equation follows the standard multivariate regression form (5.9). (Wold et al., 2001)

The idea of PLS is to find such latent variables $\boldsymbol{T}$ that maximally describe the covariance of $\boldsymbol{X}$ and $\boldsymbol{Y}$ with respect to the number of latent variables l. Thus, PLS provides the means to capture the predictor and response covariance by using the minimal number of latent variables. As a result, the obtained regression model remains as simple as possible. (Höskuldsson, 1988)

The calculation of a PLS model can be realized either with the NIPALS algorithm or with a kernel algorithm (Dayal and MacGregor, 1997b; Lindgren and Rännar, 1998). NIPALS (Wold et al., 2001) is the classical method introduced by Wold (1965) and involves an iterative calculation of the latent structure from the predictor and response data matrices (except in the special case where $m = 1$). The typical version of the NIPALS algorithm is given for example by Wold et al. (2001).

The kernel algorithms, on the contrary, replace the iteration by calculation of the eigenvalues of covariance matrix products (Lindgren and Rännar, 1998). The idea was originally presented by Höskuldsson (1988), and some of the first actual kernel algorithms were published by Glen et al. (1989a,b) and Lindgren et al. (1993). According to Lindgren et al. (1993) the first PLS predictor weight vector $\boldsymbol{w}_1^*$ is obtained as the main eigenvector of $\hat{\boldsymbol{R}}_{\boldsymbol{xy}}\hat{\boldsymbol{R}}_{\boldsymbol{xy}}^T$, and the first response weight $\boldsymbol{c}_1$ as the main eigenvector of $\hat{\boldsymbol{R}}_{\boldsymbol{xy}}^T\hat{\boldsymbol{R}}_{\boldsymbol{xy}}$. After determining the first PLS latent direction, the

covariance matrices have to be deflated before calculating the next latent direction. It has been shown that less computations are needed in the kernel approach than in NIPALS, meaning that the computational speed of the kernel algorithm is faster (Dayal and MacGregor, 1997a; De Jong and Ter Braak, 1994; Lindgren et al., 1993).

The typical structures of NIPALS and kernel based PLS algorithms are given in Table 5.1. Both algorithm versions start with the initialization of the data structures. After that, the vectors spanning the latent variables are calculated one by one in a sequential manner. The data structures are deflated by subtracting the effect of the previously obtained latent variables before the next latent variable is computed. Finally the PLS model is obtained from the PLS loadings.

Table 5.1: Comparison of the structure of NIPALS and kernel approaches for PLS calculation (based on Dayal and MacGregor (1997a)).

NIPALS-based approach	Kernel approach
1. Preprocess the data in $\boldsymbol{X}$ and $\boldsymbol{Y}$. 2. Initialize $\boldsymbol{X}_1 \leftarrow \boldsymbol{X}$ and $\boldsymbol{Y}_1 \leftarrow \boldsymbol{Y}$ 3. For each latent variable $i = 1, \ldots, l$: (a) Compute the i:th PLS weights ($\boldsymbol{w}_i^*$, $\boldsymbol{c}_i$), loadings ($\boldsymbol{p}_i$) and scores ($\boldsymbol{t}_i$) iteratively from $\boldsymbol{X}_i$ and $\boldsymbol{Y}_i$. (b) Deflate at least $\boldsymbol{X}_i$ by subtracting the effect of computed latent vectors, and substitute the result to $\boldsymbol{X}_{i+1}$. $\boldsymbol{Y}_i$ can either be deflated as well or substituted as such to $\boldsymbol{Y}_{i+1}$. (c) Go to step 3a to compute the next latent variable. 4. Calculate the final PLS mapping as $\boldsymbol{B}_{\mathrm{PLS}} = \boldsymbol{W}^*\boldsymbol{C}^T$.	1. Preprocess the data in $\boldsymbol{X}$ and $\boldsymbol{Y}$. 2. Calculate the covariance matrices $\hat{\boldsymbol{R}}_{\boldsymbol{x}}$ and $\hat{\boldsymbol{R}}_{\boldsymbol{xy}}$. 3. Initialize $\hat{\boldsymbol{R}}_{\boldsymbol{x}}^1 \leftarrow \hat{\boldsymbol{R}}_{\boldsymbol{x}}$ and $\hat{\boldsymbol{R}}_{\boldsymbol{xy}}^1 \leftarrow \hat{\boldsymbol{R}}_{\boldsymbol{xy}}$. 4. For each latent variable $i = 1, \ldots, l$: (a) Compute the i:th PLS weights ($\boldsymbol{w}_i^*, \boldsymbol{c}_i$) and loadings ($\boldsymbol{p}_i$) with a kernel algorithm e.g. using the eigenvalue decomposition of $\hat{\boldsymbol{R}}_{\boldsymbol{xy}}^T\hat{\boldsymbol{R}}_{\boldsymbol{xy}}$ and the predictor covariance $\hat{\boldsymbol{R}}_{\boldsymbol{x}}$. (b) Deflate $\hat{\boldsymbol{R}}_{\boldsymbol{x}}^i$ and $\hat{\boldsymbol{R}}_{\boldsymbol{xy}}^i$ by subtracting the effect of the computed latent vectors and substitute the result to $\hat{\boldsymbol{R}}_{\boldsymbol{x}}^{i+1}$ and $\hat{\boldsymbol{R}}_{\boldsymbol{xy}}^{i+1}$. (c) Go to step 4a to compute the next latent variable. 5. Calculate the final PLS mapping as $\boldsymbol{B}_{\mathrm{PLS}} = \boldsymbol{W}^*\boldsymbol{C}^T$.

As mentioned above, the NIPALS iteration is avoided by the kernel algorithm. However, step 4a (Table 5.1) of the kernel approach (computing of the PLS loadings) requires the calculation of the largest eigenvector of a covariance matrix product (Lindgren et al., 1993). This typically involves the power method or a singular value decomposition (SVD) algorithm (Dayal and MacGregor, 1997a).

After initialization, the kernel version uses only the covariance matrices, whereas NIPALS requires the actual data matrices. This is an advantage of the kernel method,

especially if the number of data samples N is large compared to the data dimensions (n and m), because computing with the small covariance matrices is faster and less memory consuming than dealing with the large data matrices. Kernel algorithms optimized for large dimensions and small number of data samples have been presented as well (Rännar et al., 1994, 1995).

Another advantage of the kernel approach is the easy implementation of a recursive PLS algorithm. This fact is essential for the applications presented in this thesis, and it is further discussed in Section 5.3.

More recently, Trygg and Wold (2002) have enhanced the PLS approach by combining it with orthogonal signal correction (OSC) preprocessing (Wold et al., 1998) (see Section 5.4.2) to increase the interpretability of the regression model. The idea of the orthogonal projections to latent structures (OPLS) algorithm is to separate the variation in $\boldsymbol{X}$ that is orthogonal to $\boldsymbol{Y}$ (and thus, is not explaining $\boldsymbol{Y}$) before calculating the PLS model. This simplifies the PLS model and improves the data analysis since the non-correlated part of $\boldsymbol{X}$ can be separately examined. Furthermore, an extension of the OPLS named kernel-based orthogonal projections to latent structures (K-OPLS) has been published by Rantalainen et al. (2007). K-OPLS utilizes the kernel approach of PLS to deal with nonlinear data.

5.2.4 Local Modeling

The utilization of local models in multivariate regression is a vast and vaguely defined field of data-based modeling. In most cases the idea is to compensate for nonlinearities in the data by dividing both the predictor and response space into regions where linearity assumption approximately holds (Pérez-Marín et al., 2007).

Local modeling methods are in this study classified in two main categories: A) methods utilizing a database and ad hoc modeling; B) methods utilizing a set of precalculated local models. In type A methods, a database of predictor and response samples is maintained. For each new unknown predictor, the most similar (i.e. closest) predictor samples in the database are selected into a training data set, and a local regression model $\boldsymbol{B}_{\text{local}}$ is estimated based on them. The model is then utilized in (5.10) to predict the response for that sample. In type B methods, a set of local models $\boldsymbol{B}_1, \boldsymbol{B}_2, \ldots, \boldsymbol{B}_{N_{\text{local}}}$ is calculated to cover the global data space. When a prediction is needed, a weighted average of the local model predictions is calculated. Figure 5.1 illustrates the point.

The type A local modeling methods have been more common in NIR spectroscopy (Davies and Fearn, 2008; Pérez-Marín et al., 2007) than those of type B. The first algorithm that utilized local modeling for NIR data was CARNAC (Davies et al., 1988), where the new prediction was calculated as a weighted average of the training set responses. Additionally, Fourier transformation was used to compress the spectral information in order to improve the speed of the calculation. A more sophisticated version of the algorithm (CARNAC-D) was developed more recently (Davies and Fearn, 2008). Locally weighted regression (LWR) was introduced by Cleveland (1979) as a data smoothing method, and then combined with PCR for usage in local modeling (Naes and Isaksson, 1992; Wang et al., 1994). The training set selection in LWR is

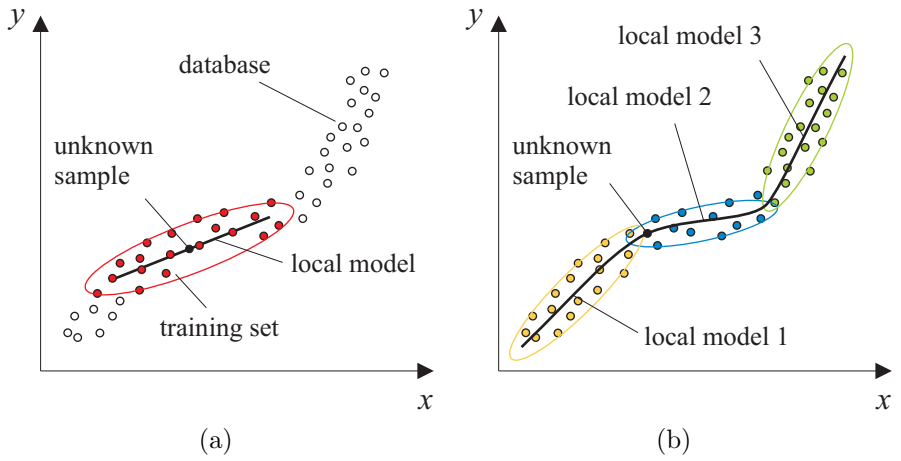

Figure 5.1: (a) Type A local modeling methods calculate a new local regression model for each unknown predictor, whereas (b) type B methods use a pre-calculated set of local regression models.

performed in the PCR score space, which improves the modeling results. Local PLS models are utilized in LOCAL, a commercially available local modeling approach specially designed for NIR data (Shenk and Westerhuis, 1997). Finally, locally-biased regression combines PLS and OSC to determine a local bias-correction for a global PLS model (Fearn and Davies, 2003).

Local modeling in a more general application field have extensively been discussed by Atkeson et al. (1997), who use the term "lazy learning" to describe type A local modeling methods. The word "lazy" refers to the fact that the model is computed only when a new prediction has to be calculated.

The disadvantages of type A local methods are that a large database has to be maintained and that the prediction model has to be estimated every time a new prediction is calculated. The type B local modeling methods avoid both of these problems by calculating the local models in advance. This involves proper clustering of the data, which can be performed by a suitable algorithm (see e.g. Barakat et al. (2004); Naes and Isaksson (1991); Shen et al. (2004)). For each cluster, a simple regression model (e.g. PCR or PLS) is calculated and the models as well as their locations in the data space are stored. A new prediction is obtained by calculating the relevance or validity of each local model with respect to the new predictor in the predictor space, and then weighting the local model predictions accordingly.

In addition to chemometrical applications (Barakat et al., 2004), type B local methods have been utilized for control engineering as well (Murray-Smith and Johansen, 1997). In particular, Schaal and Atkeson (1998) and Vijayakumar et al. (2005) have developed iterative local data learning algorithms for high-dimensional robot control.

In Publications **III** and **IV**, type A and B local modeling methods, respectively, are applied to the modeling of the VNIR reflectance spectral data. However, there the motivation for local modeling stems from the adaptive updating of the calibration model instead of data nonlinearities.

5.3 Recursive Identification

The multivariate modeling methods in Section 5.2 were presented in batch or off-line mode, meaning that a set of data $\{\boldsymbol{X}, \boldsymbol{Y}\}$, or the covariance matrices $\boldsymbol{R}_x$ and $\boldsymbol{R}_{xy}$ calculated from the data, are assumed to be available prior to modeling. The selected model parameters are then identified and a fixed model matrix $\boldsymbol{B}$ based on the statistical properties of the whole data set is obtained. However, especially in process industry applications, one is often interested in modeling the process on-line, which involves simultaneous data collection and model calculation. Typically the statistical properties of process signals tend to change in time because process operating point, raw material properties, external factors etc. vary. Since the system is time varying and the signals are not stationary, a fixed model is not adequately describing the system for longer time periods. Instead, recursive identification is used.

Recursive identification (Ljung and Söderström, 1983) is based on the updating of the model parameters every time new data are available. General forms of recursive identification algorithms are presented and the well-known recursive least squares (rLS) algorithm is discussed in detail by Ljung and Söderström (1983) and Ljung (1999).

The recursive modeling approach presented in this thesis, however, utilizes the recursive updating of the covariance matrices with new data. From the covariances, the regression models are then calculated as presented in Section 5.2. The basic recursive algorithm for a sample covariance matrix is

$$\hat{\boldsymbol{R}}_x(k) = \hat{\boldsymbol{R}}_x(k-1) + \gamma(k)[\boldsymbol{x}(k)\boldsymbol{x}^T(k) - \hat{\boldsymbol{R}}_x(k-1)], \tag{5.24}$$

where

$$\boldsymbol{x}(1), \boldsymbol{x}(2), \ldots, \boldsymbol{x}(k), \ldots \tag{5.25}$$

is a sequence of data samples $\boldsymbol{x}$ indexed by k, $\hat{\boldsymbol{R}}_x(k)$ is an estimate of the covariance $\boldsymbol{R}_x$ after k samples and $\gamma(k)$ is a scalar gain. The recursion (5.24) follows the general form where at each step the momentary error of the estimate $(\boldsymbol{x}(k)\boldsymbol{x}^T(k) - \hat{\boldsymbol{R}}_x(k-1))$ multiplied by gain $(\gamma(k))$ is subtracted from the old estimate $(\hat{\boldsymbol{R}}_x(k-1))$ to obtain the new estimate.

5.3.1 Exponential Forgetting

The tracking of time varying statistical properties of a signal essentially involves forgetting of the old data: one wants to estimate the current value of the statistics as accurately as possible, not the average of all the previous values. The most common forgetting scheme — probably because of its easy implementation in recursive form — is the exponential forgetting. The off-line counterpart of exponential forgetting is a weighted average calculation, where the sample weights are decreasing exponentially as the sample index decreases. The sample covariance matrix estimate of the samples $\boldsymbol{x}(1), \boldsymbol{x}(2), \ldots, \boldsymbol{x}(k)$ with exponential forgetting is

$$\hat{\boldsymbol{R}}_x(k) = \left[\sum_{i=1}^{k} \lambda^{k-i}\right]^{-1} \sum_{i=1}^{k} \lambda^{k-i} \boldsymbol{x}(i)\boldsymbol{x}^T(i). \tag{5.26}$$

The scalar forgetting factor λ, $0 < \lambda < 1$, is typically selected slightly smaller than one.

The recursive form of the weighted sum (5.26) equals to the selection of gain as

$$\gamma(k) = \frac{1-\lambda}{1-\lambda^k} \tag{5.27}$$

in (5.24). After the initial transient $k \gg 0$, and the gain can be approximated by a constant value $\gamma(k) \approx \gamma = 1 - \lambda$. This results in the recursive form

$$\begin{aligned} \hat{\boldsymbol{R}}_x(k) &= \hat{\boldsymbol{R}}_x(k-1) + (1-\lambda)[\boldsymbol{x}(k)\boldsymbol{x}^T(k) - \hat{\boldsymbol{R}}_x(k-1)] \\ &= \lambda\hat{\boldsymbol{R}}_x(k-1) + (1-\lambda)\boldsymbol{x}(k)\boldsymbol{x}^T(k), \end{aligned} \tag{5.28}$$

as given in (Ljung, 1999). In some cases only the structure of the covariance matrix is of importance, and the scaling can be omitted. For example, the eigenvector directions used in PCA and PLS remain the same regardless of the scaling. The unscaled exponentially weighted covariance estimate is (Ljung, 1999)

$$\hat{\overline{\boldsymbol{R}}}_x(k) = \sum_{i=1}^{k} \lambda^{k-i}\boldsymbol{x}(i)\boldsymbol{x}^T(i), \tag{5.29}$$

which corresponds to the simple recursion

$$\hat{\overline{\boldsymbol{R}}}_x(k) = \lambda\hat{\overline{\boldsymbol{R}}}_x(k-1) + \boldsymbol{x}(k)\boldsymbol{x}^T(k). \tag{5.30}$$

The scaled and unscaled estimates of the cross-covariance matrix $\boldsymbol{R}_{xy}$ are correspondingly updated by replacing $\boldsymbol{x}(k)\boldsymbol{x}^T(k)$ with $\boldsymbol{x}(k)\boldsymbol{y}^T(k)$ in (5.28) and (5.30).

Recursive exponential forgetting can be used more generally as a low-pass filter for an arbitrary signal a:

$$a_{\text{filt}}(k) = \lambda a_{\text{filt}}(k-1) + (1-\lambda)a(k). \tag{5.31}$$

The effect of the selected forgetting factor can be evaluated by calculating the memory time constant:

$$T_0 = \frac{1}{1-\lambda}. \tag{5.32}$$

T_0 describes how long (in sampling intervals) the system is assumed to remain constant. (Ljung, 1999)

5.3.2 Recursive Partial Least Squares

Recursive calculation of the LS, PCR and PLS regression models with exponential forgetting can in principle be realized by combining the (scaled or unscaled) recursive updating of the covariance matrices (Equations (5.28) or (5.30)) with the kernel algorithms of the respective regression models presented in Section 5.2. However, this approach is not truly recursive in the sense that every updating step requires the calculation of a new regression model from the covariances. For the least squares model,

the common rLS algorithm with efficient matrix inversion (Ljung, 1999) should be used instead. For recursive PCR (rPCR) or PCA (rPCA), the suggested framework requires computationally intensive calculations after each updating step as well. One first needs to perform the eigenvalue decomposition of the covariance (for PCA) and then to compute the matrix product (5.20) including a matrix inversion. In the literature, several alternative algorithms for recursive PCA with improved computational properties have been presented (Erdogmus et al., 2004; Li et al., 2000). If the computational efficiency is of importance, then these algorithms provide a better starting point for rPCR.

Recursive PLS (rPLS) is, however, typically realized by the presented approach, where the covariance matrices are updated recursively and a kernel method is then used to obtain the final mapping matrix $\boldsymbol{B}_{\mathrm{PLS}}$ (Dayal and MacGregor, 1997b; Miletic et al., 2004). Initially, recursive calculation of PLS was proposed by Helland et al. (1991), whose idea was to augment a fixed size representation of the old data with the new data, and then to apply NIPALS to these augmented matrices. Qin (1993, 1998) improved the algorithm by introducing on-line adaptation with a moving window and exponential forgetting, block-wise adaptation and application principles to dynamic and nonlinear regression. At the same time, the rPLS algorithm based on recursively updated covariance matrices and kernel PLS was presented by Dayal and MacGregor (1997a,b). The algorithm utilizes the unscaled covariance matrix recursion (5.30) and the improved kernel PLS algorithm (Dayal and MacGregor, 1997a). Separate mean-centering of the variables is avoided in the algorithm by augmenting the predictor data with a constant variable:

$$\tilde{\boldsymbol{x}} = \begin{bmatrix} \boldsymbol{x}^T & 1 \end{bmatrix}^T, \tag{5.33}$$

and by using the augmented data instead of the original. This kind of mean-centering is a standard method in linear regression (Gemperline, 2006; Martens and Næs, 1989), and when combined to recursive regression methods it provides a compact way to adaptively compensate for the effect of the possibly changing data mean.

In this thesis, the rPLS algorithm by Dayal and MacGregor (1997a) is used as the main regression method in Publications **II**–**VII**, and the adaptive mean-centering is utilized in Publications **II** and **VII**.

5.4 Data preprocessing

The aim of data preprocessing is to improve the modeling performance by modifying the measured data before model calculation. When dealing with linear regression model structures, one purpose of the preprocessing is to linearize the relationship between predictors and responses. Another important aim is to eliminate from data such variation that is unrelated to the modeling problem at hand.

5.4.1 Linearity Pursuit

There are two main methods to handle the nonlinear relationship of the predictor and response data: 1) applying a nonlinear transformation to the predictor and/or

response data, or 2) using extra predictor variables (Martens and Næs, 1989). In spectroscopy, the nonlinear transformation can be selected based on theoretical models for the specific measurement setup. A common transformation in diffuse reflectance spectroscopy is to use the absorbance $\log(1/R)$ instead of the measured reflectance R. This is motivated by the linear relationship (3.5) between the absorbent concentration and the absorbance derived from the Beer-Lambert law (Norris, 1983; Osborne et al., 1993). The $\log(1/R)$ transformation is used in Publications **III**, **IV**, **V** and **VII**. Another theory-based transformation for linearity is the Kubelka-Munk function (3.8).

5.4.2 Preprocessing Methods

Generally, the most basic preprocessing of multivariate data includes mean-centering and variance normalization of each predictor and response variable. Especially for PCR (or PCA), the mean-centering of the predictor data is typically essential. If the mean-centering is omitted, the data mean dominates the direction of the first PC and affects the rest of the PCs as well (see e.g. Li et al., 2000).

In the field of spectroscopy, common preprocessing techniques are standard normal variate (SNV) and multiplicative scatter correction (MSC). Both of the methods are meant to reduce the data variance caused by scattering effects (Fearn et al., 2009; Gemperline, 2006). SNV is based on normalization of each spectrum by standardizing each intensity value, that is, by subtracting the sample mean intensity of the spectrum and dividing the result by the sample standard deviation of the intensities. MSC (Fearn et al., 2009; Geladi et al., 1985), on the other hand, normalizes the spectra by compensating for the additive and multiplicative effects caused by scattering. Other popular preprocessing methods for spectral data include the calculation of first and second derivative, baseline correction and smoothing (Gemperline, 2006; Martens and Næs, 1989).

All the abovementioned preprocessing methods are based on the modification of the measured spectral data $\boldsymbol{X}$ independent of the corresponding responses $\boldsymbol{Y}$. Since the aim of the analysis is to model $\boldsymbol{Y}$ linearly from $\boldsymbol{X}$, a natural starting point for preprocessing would be to only remove such variation from $\boldsymbol{X}$ that is not explaining $\boldsymbol{Y}$. This idea was proposed by Wold et al. (1998), who also named it as orthogonal signal correction (OSC). In the original OSC, the NIPALS algorithm is applied to finding the largest variance directions in $\boldsymbol{X}$ that are as orthogonal as possible to $\boldsymbol{Y}$. The most important such directions are then removed from $\boldsymbol{X}$ and the resulting data are further used in model calculation, usually by PLS.

Several variations of the original OSC algorithm have been presented, for example by Sjöblom et al. (1998), Anderson (1999), Fearn (2000) and Westerhuis et al. (2001). Furthermore, the same idea is utilized in the O-PLS and K-OPLS algorithms (see Section 5.2.3). Some of the OSC algorithms were tested and compared by Svensson et al. (2002). They showed that OSC preprocessing does not significantly improve the prediction performance if PLS is used for the actual modeling. However, the removal of OSC components leads to simpler PLS models, because less latent variables are required to reach the same prediction error. Additionally, the interpretation of the

model is improved since also the uncorrelated variance captured by OSC can be analyzed. These benefits are obtained by the O-PLS algorithm as well (Trygg and Wold, 2003).

The OSC algorithm proposed by Fearn (2000) is used as the starting point in Publication **IV**, where a kernel version of OSC is derived. The kernel OSC is further combined to the recursively updated covariance matrices to obtain a recursive OSC preprocessing algorithm.

5.5 Model Evaluation and Validation

The quality of an estimated regression model should be evaluated with respect to the intended usage. Usually the aim in regression is to predict the response of new predictor samples without knowing the real response values. In such a case, a natural method to evaluate the model quality is to measure the error between the predictions $\hat{\boldsymbol{y}}$ and measured predictors $\boldsymbol{y}$:

$$\hat{\boldsymbol{e}} = \boldsymbol{y} - \hat{\boldsymbol{y}}. \tag{5.34}$$

Model validation is typically based on the estimation of the statistical properties of the estimation error (5.34) from a validation data set. The standard criterion used is the mean square error (MSE) (Martens and Næs, 1989), which is the sample average of the squared estimation errors:

$$\mathrm{MSE}_i = \frac{1}{N}\sum_{i=1}^{N} \hat{e}_i^2(k), \quad i = 1, \ldots, m, \tag{5.35}$$

where i indexes the m output variables. MSE can be divided into two parts: error caused by random variation (sample variance of $\hat{\boldsymbol{e}}$) and the systematic error (squared sample mean or bias of $\hat{\boldsymbol{e}}$). Typically also the square root of MSE, root mean square error (RMSE), is calculated. If the bias term is neglected, RMSE corresponds to the sample standard deviation of $\hat{\boldsymbol{e}}$.

An alternative method to evaluate the model is to measure the proportion of response variance explained by the predicted values. This coefficient of determination is denoted by R^2 and calculated as

$$R_i^2 = 1 - \frac{\sum \hat{e}_i^2(k)}{\sum (y_i - \mu_{y_i})^2}, \quad i = 1, \ldots, m, \tag{5.36}$$

where μ_{y_i} is the average of y_i (Wold et al., 2001). In the case of crossvalidation, that is, when separate data sets are utilized for model estimation and validation, the coefficient of determination for the validation data is denoted by Q^2 (Wold et al., 2001).

5.6 Singular Spectrum Analysis

Singular spectrum analysis (SSA) (Golyandina et al., 2001) differs from most of the other data-based methods presented in this chapter because it is used to analyze time

series data. However, the idea of PCA is strongly incorporated into the calculation of SSA as shown below. SSA decomposes the original time series into orthogonal components which typically represent oscillations, trends and noise of the signal. The decomposition is used to analyze the structure of the time series and to reproduce a modified version (e.g. without noise) of the original series. Forecasting based on the SSA decomposition is possible as well.

The introduction of SSA is usually connected to the publication by Broomhead and King (1986), but also earlier studies applying the same idea can be found (see e.g. Kumaresan and Tufts (1980)). SSA has been especially popular in climatology for extracting trends and oscillations from noisy signals (Rodó et al., 1997; Vautard and Ghil, 1989; Yiou et al., 1994). It is, however, utilized also in other fields like physics (Marrelli et al., 2001), economics (Hassani et al., 2009) and telecommunications (Tzagkarakis et al., 2009), to mention a few. In process industry, SSA has been applied for example to signal preprocessing in system identification (Aldrich and Barkhuizen, 2003) and to analyze the nature of process dynamics (Jemwa and Aldrich, 2006).

5.6.1 Algorithm

The basic SSA algorithm presentation given here follows mainly the one by Golyandina et al. (2001), who divide the analysis into two main stages: decomposition and reconstruction. The analyzed signal is assumed to be represented by an N samples long time series $\boldsymbol{g} = [g(1)\, g(2)\, \cdots\, g(N)]^T$.

Decomposition: The decomposition phase starts with the selection of an integer window length L, $1 < L < N$. Then all the possible sets of L consecutive samples in $\boldsymbol{g}$, that is, lagged vectors $\boldsymbol{z}^T$, are embedded as the $K = N - L + 1$ rows of the trajectory matrix $\boldsymbol{Z}$:

$$\boldsymbol{Z} = \begin{bmatrix} \boldsymbol{z}^T(1) \\ \boldsymbol{z}^T(2) \\ \vdots \\ \boldsymbol{z}^T(K-1) \\ \boldsymbol{z}^T(K) \end{bmatrix} = \begin{bmatrix} g(1) & g(2) & \cdots & g(L) \\ g(2) & g(3) & \cdots & g(L+1) \\ g(3) & g(4) & \cdots & g(L+2) \\ \vdots & & & \vdots \\ g(K) & g(K+1) & \cdots & g(N) \end{bmatrix}. \tag{5.37}$$

As a direct result of the embedding procedure, the trajectory matrix is a Hankel matrix meaning that the values on each skew diagonal are constant.

The trajectory matrix is then treated as any data matrix containing multivariate data samples: each column corresponds to a variable, and each row to a sample of an L-dimensional data vector $\boldsymbol{z}^T$. In particular, PCA (or SVD) is used to decompose the trajectory matrix into a sum of d elementary matrices according to (5.14):

$$\boldsymbol{Z} = \boldsymbol{Z}_1 + \boldsymbol{Z}_2 + \boldsymbol{Z}_3 + \ldots + \boldsymbol{Z}_d, \tag{5.38}$$

where d equals the rank of $\boldsymbol{Z}$, and each elementary matrix is the outer product of the corresponding PCA loading $\boldsymbol{p}_i$ and score $\boldsymbol{t}_i$ column vectors:

$$\boldsymbol{Z}_i = \boldsymbol{t}_i \boldsymbol{p}_i^T. \tag{5.39}$$

As a result of PCA, each loading vector $\boldsymbol{p}_i$ describes a typical L samples long structure present in the time series $\boldsymbol{g}$ and can be interpreted as an 'eigensignal'. By the nature of PCA these eigensignals are orthogonal, and arranged in a descending order according to the data variation they represent. Moreover, each lagged vector $\boldsymbol{z}(k)$ of the original time series (i.e. the whole trajectory matrix $\boldsymbol{Z}$) can be reconstructed by a linear combination of the eigensignals.

Reconstruction: As discussed by Golyandina et al. (2001), the eigensignals in SSA typically represent trend components, oscillatory components, or noise components of the original time series. In the reconstruction phase of SSA the interesting components $\{i_1, \ldots, i_p\}$ (say, the main oscillations) are grouped and used to calculate an estimate of the trajectory matrix:

$$\hat{\boldsymbol{Z}} = \boldsymbol{Z}_{i_1} + \ldots + \boldsymbol{Z}_{i_p}. \tag{5.40}$$

Finally the original signal is reconstructed by averaging the estimates of the same signal value on every skew diagonal of $\hat{\boldsymbol{Z}}$. The averages are collected as the samples of the reconstructed signal $\hat{\boldsymbol{g}}$. This last phase is referred to as diagonal averaging.

The kernel formalism used for the multivariate regression algorithms in Section 5.2 can be applied to SSA as well. The covariance that captures the necessary statistics is now the covariance matrix of the lagged vectors:

$$\hat{\boldsymbol{R}}_z = \frac{1}{K}\boldsymbol{Z}^T\boldsymbol{Z}. \tag{5.41}$$

Based on the covariance the structure (loadings $\boldsymbol{P}$) of the signal can be extracted by PCA, even though the actual trajectory matrix would not be available. This idea is further utilized in Publication **VI**, where a recursive version of SSA is derived for on-line characterization of signal structures.

Chapter 6

Measurements and Modeling

The experimental part of the research was conducted at the operational concentration plant of Pyhäsalmi Mine Oy. Mainly two types of data were collected from the flotation process: the VNIR reflectance spectral measurements of the flotation froths and slurries, and the XRF analysis of the slurries. Several prototype devices were developed for the VNIR reflectance measurements, whereas the XRF results were obtained from the XRF analyzer regularly used at the plant. Based on the analysis of the data, the information content of the VNIR spectra regarding the elemental contents of the froths and slurries was evaluated, and the XRF assays were used as reference values.

In this chapter, the background of the proposed analysis approach is discussed, and the measurement arrangements and data collection methods utilized in the publications are summarized. The application of the data analysis methods is presented as well.

6.1 Preliminary Discussion

Before reviewing the actual measurement arrangements used in the course of this research, it is worthwhile to evaluate some of the starting points for the analysis. The general optical properties of the main minerals present in the Pyhäsalmi ore (see Table 2.1) can be analyzed using database laboratory spectra. Figure 6.1 shows the hemispherical VNIR reflectance spectra of the five main minerals in two size classes drawn from the ASTER spectral library data (Baldridge et al., 2009).

Even though the spectra are from dry mineral samples, as opposed to mineral slurries or froths, some observations can be made:

- Sphalerite (the zinc-bearing mineral) and barite (gangue mineral) have generally higher reflectance than the other minerals, meaning that they should dominate the spectra of the real mineral mixtures.
- None of the minerals have sharp absorbance regions in the analyzed wavelength range, which suggests that the spectrum analysis can be focused on the overall shape of the spectra.

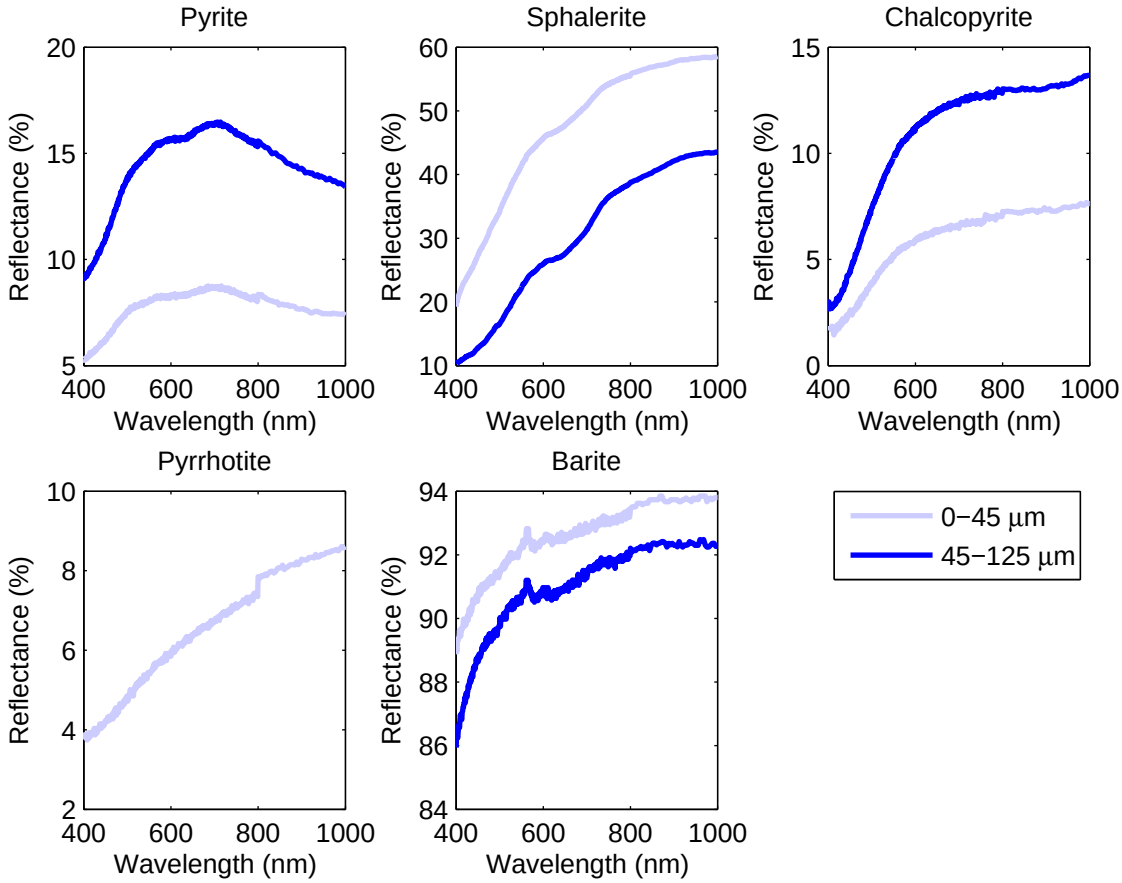

Figure 6.1: The laboratory VNIR spectra of the main minerals in two particle size classes. The data were acquired from the ASTER spectral library (Baldridge et al., 2009). For pyrrhotite, only the smaller particle size class data were available.

- Particle size affects strongly the overall reflectance of the sample. In addition, the effect is mineral dependent: in pyrite and chalcopyrite, samples with smaller particles are less reflective, whereas for sphalerite and barite the opposite is true. As a result, unknown changes of the particle size distribution disturb the spectral measurements.

The VNIR reflectance spectra of the froth and slurry samples are determined by the mineral composition of the sample, whereas the XRF analyzer is measuring the elemental contents of the slurries. Thus, in order to combine these two measurement approaches, some assumptions on the mineralogy of the sampled froths and slurries has to be made. In the case of Pyhäsalmi ore, the zinc and copper contents are in direct relationship to the amounts of sphalerite and chalcopyrite, respectively. However, the zinc/iron ratio of sphalerite affects the optical properties of the mineral, which disturbs the spectral measurement. Unknown changes of the gangue mineral concentrations and particle size distribution of the slurry feed are possible sources of error as well. Throughout the thesis, it is assumed that these changes are rather

smooth because of the mixing taking place in the comminution process preceding the flotation, so that the adaptive calibration of the spectral measurement is able to compensate for their effect.

6.2 XRF Slurry Assays

The XRF assay data for all the publications were obtained directly from the XRF analyzer of the plant (Outotec Courier® 6 SL). The structure of the analyzer is a centralized one, meaning that continuous slurry samples from the process streams are transferred to the analyzer by the primary sampling pipes. A multiplexer then samples each primary line in turn for the analysis, which is performed by a single X-ray tube and spectrometer. The assays are calculated from the measured XRF spectra using a multivariate regression model. The model calibration is based on laboratory measurements.

At Pyhäsalmi the XRF analyzer is measuring 14 slurry lines, but the most critical lines are assayed twice during the measurement cycle. This increases the sampling interval of a typical line to around 18 minutes. The secondary sampling of the analyzer lasts about 30 seconds, during which the slurry sample for the actual analysis is collected. Correspondingly, the XRF assays thus represent the elemental contents of the slurry averaged over the 30 second time period. The most important elements measured are iron, copper and zinc, as well as the solid content of the slurry. In addition, an estimate for the sulfur content is calculated from the measurement results.

6.3 Imaging VNIR spectrographs

The VNIR spectrum was measured with the Specim ImSpector V10 spectrograph connected to a monochrome CCD camera (Basler A102f). The spectrograph is based on a prism-grating-prism (PGP) structure (Aikio, 2001), which disperses the light measured from a target line to its spectral elements (Figure 6.2). The horizontal axis of the gray scale image acquired from the CCD camera corresponds to the location along the target line, and the vertical axis indicates the spectral wavelength. Thus the intensity of a pixel in the image describes the intensity of the corresponding spectral component in the light measured from a short part of the target line. A complete hyperspectral image can be obtained by sweeping the spectrograph over a target or letting the targe slide past the spectrograph (e.g. when measuring the spectra of objects that are moving on a belt conveyor).

Two spectrograph versions were utilized in the measurements performed in the publications. The first one had normal optics and was capable of measuring the spectra of a line as described above. It was used for the froth measurements in Publication **I** and in the first slurry analyzer prototype described in Publication **II** (see Section 6.5). In the second version, the optics was replaced by a fiber bundle, whose common end was attached to the spectrograph and aligned so that the fibers were located horizontally in a row. This enabled the concurrent spectral measurement

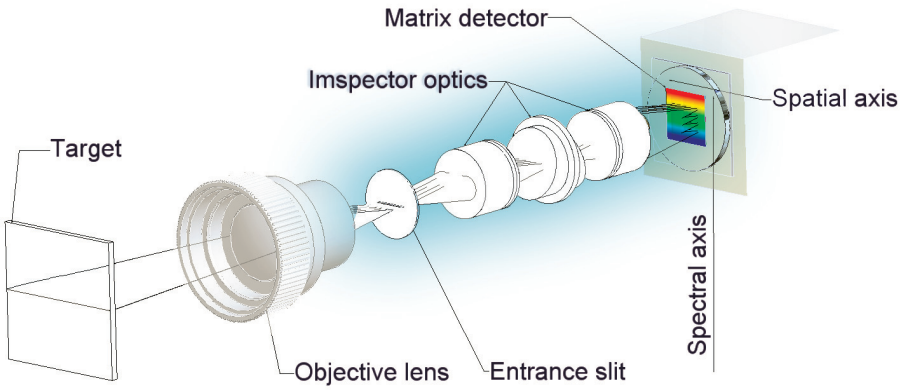

Figure 6.2: The internal structure of the prism-grating-prism imaging spectrograph. (Courtesy of Specim)

of the targets seen by each of the fibers. The fiber optic version was used in the second and third slurry analyzer prototypes described in Publications **V** and **VII** (see Section 6.5), where several slurry lines were simultaneously analyzed.

The wavelength range of both spectrographs was 400-1000 nm, and the spectral resolution 5 nm. The same CCD camera was used in both spectrographs with a resolution of 1280x960, that is, every image captured with the normal optics spectrograph contained 1280 spectra with 960 wavelength values. In the fiber optics version, each fiber covered about 25 pixel columns in the final image and contained 960 wavelength values. The CCD camera was used in the 8 bit mode, meaning that each pixel had 256 possible intensity values. The fiber optics spectrograph contained 10 fibers, each 7.5 m long and with a collimator lens in the end.

6.4 Froth VNIR Measurements

The froth analysis tests for this study were performed on the last zinc cleaner cell at the Pyhäsalmi concentration plant. The spectrum of the froth was measured using the VNIR spectrograph with normal optics, and the spectrograph was installed on top of the cell pointing directly down. The spectrograph was located next to an existing RGB froth camera (Figure 6.3), which is part of the multicamera system (Kaartinen, 2001; Kaartinen et al., 2006b) installed earlier on the concentration plant. The halogen light of the froth camera system was used to illuminate the froth also for the spectral measurements, and the spectrograph was connected to a laptop computer to store the spectra. As shown in Figure 6.3, the spectrum measurement line was positioned in the froth area measured by the RGB camera, thus ensuring that the same froth was analyzed by both spectrograph and RGB camera.

The length of the spectrograph line on the froth surface was about 30 cm, even though some variations occurred because of the changes in the height of the froth. The line length was much larger than the diameter of an average bubble, so that each captured spectrum image contained spectra from the brighter bubble centers as well

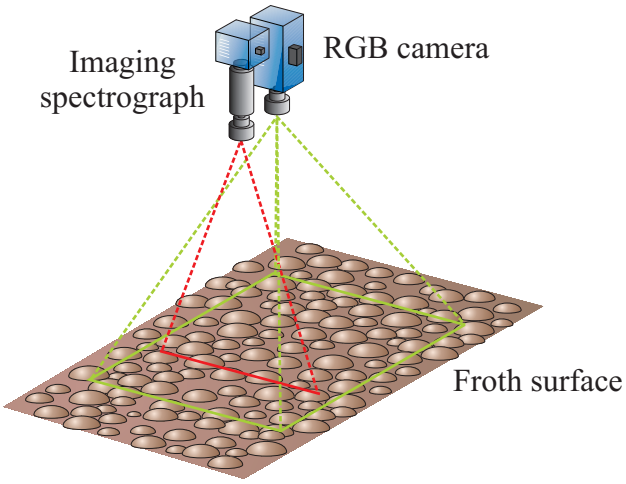

Figure 6.3: The spectrograph was installed next to an existing RGB froth camera on top of the final zinc cleaning cell.

as from the darker regions between the bubbles. Thus an average of the spectra in one captured image provided a good estimate of the momentary average spectrum of the froth.

The froth spectrum measurement and analysis is discussed in Publication **I**. Besides Publication **I**, an initial report of the measurement setup and of the preliminary results is given by Kaartinen et al. (2006a).

6.5 Slurry VNIR Measurements

After the initial laboratory tests described in Publications **I** and **II**, the spectrum of the mineral slurries was measured on-line from the real process streams at the Pyhäsalmi concentration plant. The slurry measurement system was gradually developed during the work described in this thesis, and three prototypes are presented in the following.

6.5.1 Prototype I

The first on-line VNIR spectral measurements of the slurry were conducted using the imaging spectrograph with normal optics. An additional slurry flow was continuously sampled from the primary sampling flow of the XRF analyzer at the concentration plant and led through a jet flow cell with a sapphire window as presented in Figure 6.4. The cell was designed to create a turbulence in the slurry flow so that a representative sample was presented in front of the window at all times. A similar kind of cell is used in the Courier® analyzers to present the sample for the XRF analysis.

The primary sample flow of the XRF analyzer is a continuous slurry flow that is sampled from the corresponding process flow (Figure 6.4). A simple vertical cutter sampler was used to fork the small continuous side flow for the spectral analysis from one of the the primary sample flows. While the typical flow rate in the primary

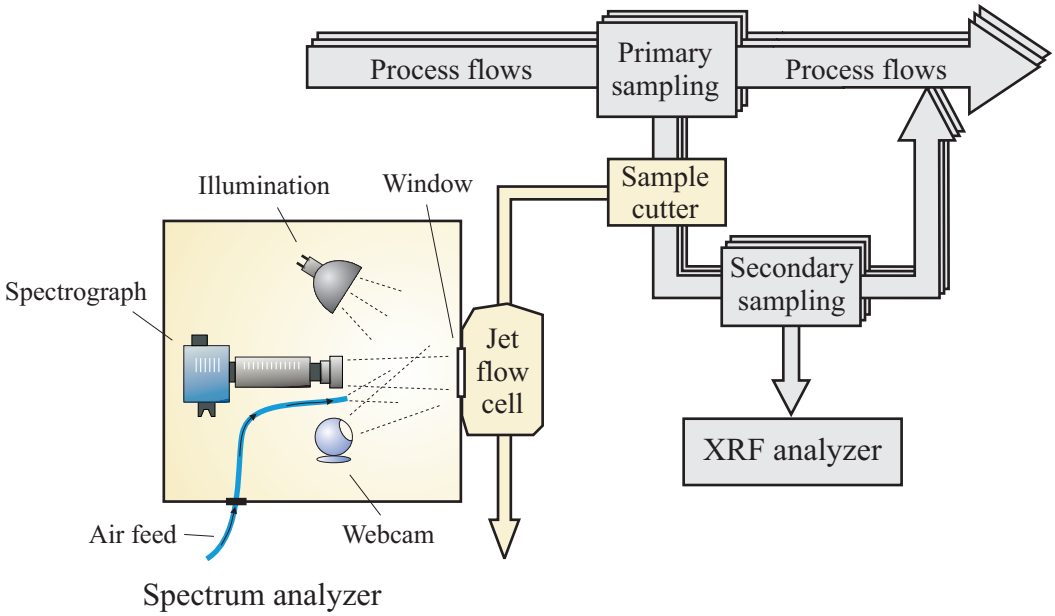

Figure 6.4: The first (single-channel) slurry measurement prototype. An additional slurry flow was sampled from one of the primary sample flows of the XRF analyzer, and the slurry was analyzed through the jet flow cell window.

sample loop of the XRF analyzer is about 200–400 l/min, the rate of the spectral jet flow cell side flow was about 60 l/min.

The spectral measurement system consisted of the imaging spectrograph, a 12 V halogen lamp and a web camera which was used to remotely monitor the flow conditions in the jet flow cell. Additionally, a small dry instrument air feed was directed to the cell window to prevent condensation. The measurement geometry was arranged so that the spectrograph was pointed perpendicularly to the cell window, whereas the illumination light angle was about 45° to reduce reflections from the glass of the window. The measurement instruments and a desktop computer were installed in a slightly over-pressurized protective housing to prevent the mineral dust and slurry splatters from disturbing the measurements.

A more detailed description of the first prototype is given in Publication **II**. Data measured by the prototype are analyzed and reported in Publications **II**, **III** and **IV**.

6.5.2 Prototype II

In the second slurry measurement prototype, the VNIR spectrum measurement was extended to cover several slurry lines simultaneously, that is, a multi-channel measurement was obtained. The prototype utilized the fiber optic version of the imaging spectrograph. Sample cutters were installed into altogether seven slurry lines right before the secondary sampling (multiplexer) of the XRF analyzer, and the sampled slurry was analyzed using individual jet flow cells. A small measurement box containing a collimator lens, halogen lamp, web camera and air feed was attached to each

jet flow cell as shown in Figure 6.5. One branch of the spectrograph fiber bundle was connected to each collimator lens so that a single spectral image contained the spectra of all the seven slurry lines.

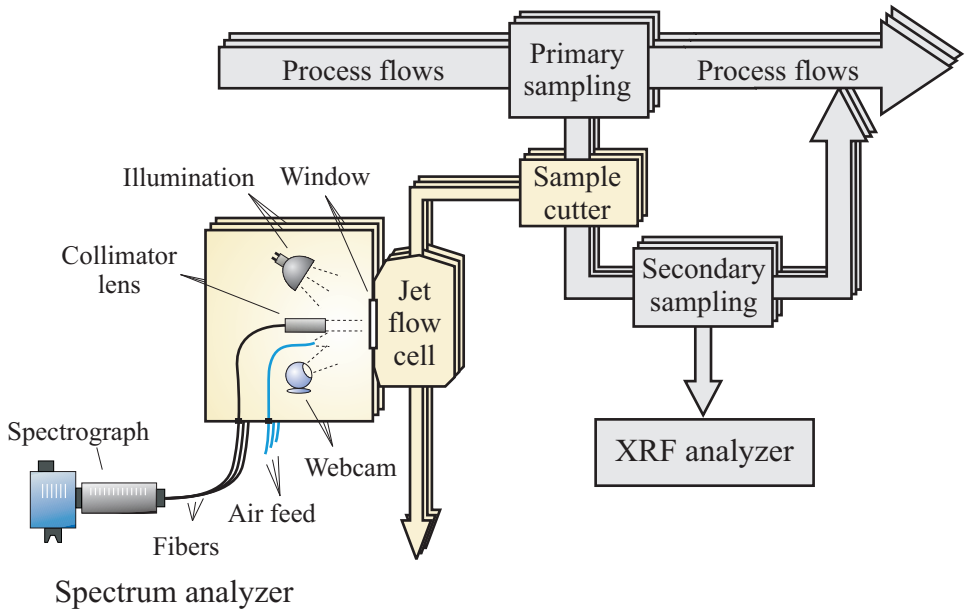

Figure 6.5: The second (multi-channel) slurry measurement prototype.

The internal structure of the measurement box was quite similar to prototype I, except that the spectrograph was replaced by the collimator lenses connected to the fibers. The collimator lenses were selected so that they captured the light reflected from the center area of the round cell windows. In this prototype, silver coated reflector halogen lamps (Osram Ministar) were utilized to maximize the amount of infrared illumination.

The halogen lights were connected to adjustable voltage sources so that the overall intensity of the reflected light could be set to the same level in all slurry lines. This was important since the common CCD sensor in the spectrograph was used to capture all the spectra, and large differences in the intensities would have reduced the numerical accuracy of the measurements.

The second prototype is described in Publication **V** and the data measured by it are utilized in Publications **V** and **VI**.

6.5.3 Prototype III

The third slurry measurement prototype was developed to prevent the blockages that occurred in prototype II because of the small sample flows. The additional sampling of the slurry was omitted, and instead a larger jet flow cell was designed and installed directly to the primary sample flow of the XRF analyzer (Figure 6.6). This structure has two advantages: 1) the blockage problems caused by the extra sampling and the small flow rates through the jet flow cells are avoided, and 2) the analyzed sample is more representative since one sampling stage is omitted.

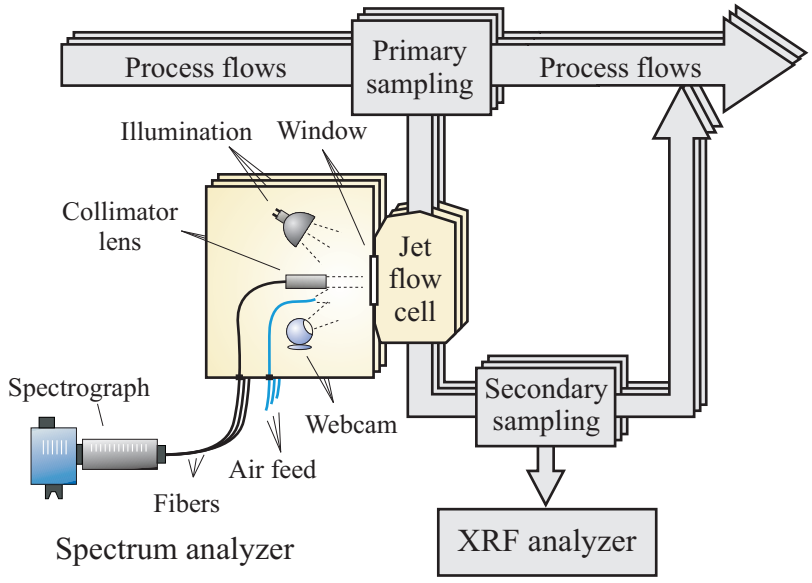

Figure 6.6: The third slurry measurement prototype, where the jet flow cells are installed directly to the primary slurry flows (Publication **VII**).

The third prototype is described and applied in Publication **VII**. It is currently in use at the Pyhäsalmi concentration plant as well.

6.6 Data Analysis

All the publications related to this thesis are based on analysis of data measured from the Pyhäsalmi concentration process. In Publications **I**–**V** and **VII**, multivariate regression is used to predict the elemental contents of the slurries, and in Publication **VI** time series of the concentration process measurements are analyzed by a new recursive singular spectrum analysis algorithm in order to detect plant-wide oscillations.

6.6.1 Multivariate Regression

The mineral flotation froth and slurry spectra are analyzed in this thesis mainly by multivariate regression methods. Especially the connection between the VNIR spectra and the elemental grades obtained from the XRF analyzer is modeled by several regression techniques typically based on PLS. The aim and basic setting of the modeling problem remains quite similar throughout the work: The fast spectral measurements of froth or slurry are used as predictors and the sparse XRF samples as the response data. For model estimation, the spectral samples corresponding to the XRF assays are collected by assuming a constant delay between the XRF and VNIR measurements, and the model is either directly or recursively estimated from these predictor-response pairs. The regression model is then applied to the rest of the VNIR spectra to predict the elemental grade changes between the XRF assays.

The froth spectra in Publication **I** are modeled by the standard PLS, even though the model is periodically recalculated from a fixed number of latest measurements. This compensates for the nonstationarity that was detected in the measured data. Recursive and static modeling are compared for slurry spectrum analysis in Publications **II** and **IV**, and the rest of the publications use solely recursive models.

The most common modeling method is recursive PLS, which is realized by recursive updating of the data covariance matrices and the kernel PLS algorithm (Dayal and MacGregor, 1997a) as explained in Section 5.3. The covariance matrices are updated with exponential forgetting after each new XRF sample is received, and a new PLS model is calculated from the updated covariances. The new model is used to predict the grades from the VNIR spectra until the next XRF sample is available. This approach was detected to work well especially for predicting the final concentrate grades, and it is utilized in Publications **II** and **V**–**VII**.

Recursive updating with exponential forgetting is only suitable for data with representative variation. In mineral flotation some elemental grades, however, stay normally very low for long periods, and increase significantly only in the case of a failure in the flotation process as wrong minerals are left to the slurry. The prediction of these sudden changes is important from the control point of view, since they typically indicate either loss of valuable minerals or decrease of the final product grade. To improve the detection of the process failure cases, two alternative modeling methods based on local modeling were developed in Publications **III** and **IV**.

The first new modeling approach (continuous locally weighted regression, CLWR) presented in Publication **III** is based on type A local modeling (see Section 5.2.4), where a calibration database is stored. Every time a new prediction is required, a subset of data is selected and a new PLS model is estimated. Adaptation to statistical changes is performed by on-line updating the database. Instead of discarding the oldest data, however, the diversity of the database is maintained by replacing one of the two most similar database samples with the new sample. This ensures that the database covers the whole response range at all times. To improve the sample selection process, OSC preprocessing is applied to the data. The details of the CLWR algorithm can be found in Publication **III**.

Type B local modeling is utilized in the second new modeling approach for the process failures, as presented in Publication **IV**. The algorithm is based on local recursive OSC and PLS models and named as recursive multimodel (rMM) approach. Separate local rPLS models are reserved for the normal operation and for the process failures, and the models are updated with the corresponding data based on the response values. Gaussian weighting functions linked to each local model indicate how important each calibration sample is when updating the model. Correspondingly, the weighting is also used when the rMM prediction is calculated as the weighted average of the local model predictions. The prediction weight is determined as the Mahalanobis distance between the model center and the query point in the OSC preprocessed predictor space.

CLWR and rMM algorithms utilize local modeling in a novel way. Instead of compensating for data nonlinearities, which typically is the motivation for a local modeling approach, the data space is now divided to local regions in order to prevent

the forgetting of the rare but locally different data samples. At the same time, the models are adaptively updated. The closest match to the rMM algorithm in the literature is the locally weighted projection regression (LWPR) algorithm presented by Vijayakumar et al. (2005), which utilizes local PLS models as well. The LWPR algorithm is, however, meant for very high dimensional data and primarily targeted for highly nonlinear problems.

The usage of the multivariate regression methods in the publications is summarized in Table 6.1. It is evident that the rPLS approach is mostly used because of its simplicity and good performance especially on the large elemental grades of the final concentrates.

Table 6.1: The usage of the different multivariate regression methods in the publications. In Publication **VI**, data produced by the rPLS are used as the starting point for the oscillation analysis.

	LS	PLS	rPLS	CLWR	rMM
Publication **I**	x	x			
Publication **II**		x	x		
Publication **III**			x	x	
Publication **IV**		x	x		x
Publication **V**			x		
Publication **VI**			(x)		
Publication **VII**			x		

6.6.2 Oscillation Analysis

Data-based detection of oscillations from industrial process signals is often performed off-line using autocorrelation functions or Fourier transformations of the signals (e.g. Hägglund, 1995; Thornhill and Hägglund, 1997; Thornhill et al., 2003, 2002; Xia et al., 2005). For the on-line analysis of copper circuit signal structures in Publication **VI**, a new algorithm named recursive singular spectrum analysis (rSSA) is developed. It combines the ordinary SSA (Section 5.6) with exponential forgetting (Section 5.3.1). The main idea of the rSSA algorithm is to maintain an up-to-date SSA decomposition of the concentration process signals on-line. A possible oscillatory period of a signal is indicated by small changes in the signal structure, and the other signals oscillating in the similar way are assumed to share the same SSA structure.

Chapter 7

Results

The main results in this thesis are related to the analysis of the froth and slurry VNIR reflectance spectra. Especially the determination of slurry elemental contents from the VNIR measurements are investigated. The main application of the spectral measurement is the high-frequency slurry assay that is obtained by combining the VNIR measurements with the sparse XRF assays. This chapter summarizes the results obtained in the publications.

7.1 Froth Analysis

The froth analysis reported in Publication **I** is one of the first studies where VNIR reflectance spectroscopy is utilized in assaying mineral froths. The main result in the publication is that the elemental contents of the zinc concentrate slurry predicted from the VNIR spectra are more accurate than the predictions from the RGB data obtained by a regular camera. However, the difference is small for iron and zinc, whereas the VNIR spectra clearly improve the prediction of the copper content.

As stated in Publication **I**, the problem with the used measurement setup is that only the froth from one of the four final zinc concentration cells is measured by the spectrograph, while the XRF analyzer assays the whole concentrate stream where the concentrates from all the four cells are mixed. Depending on the conditions in the cleaner cells their froth grades may differ, which obviously disturbs the comparison of the VNIR spectra and XRF results.

Another difficulty is the rather long temporal and spatial distance between the two measurements. As it turned out later with the slurry VNIR measurements (Publication **II**), the slurry grades typically contain high-frequency variations with a considerable amplitude. This means that the precise synchronization of the VNIR and XRF measurements is of utmost importance in order to form an accurate model for the slurry grades. However, the measurement setup used in Publication **I** prevents the proper determination of the time delay between the VNIR and XRF analyzers, since the zinc concentrate is transferred through slurry pipes and a pump sump before it is sampled for the XRF assay. In addition, the changing slurry flow speed causes the delay to vary.

The froth study in Publication **I** presents also the factor loadings of the PLS model used. It is detected that all the main loadings are smooth with respect to the wavelength, which indicates that the overall shape of the spectrum is more important than some specific narrow wavelength ranges in determining the elemental grades. This is in agreement with the visual inspection of the dry mineral spectra in Section 6.1. However, as many as six latent variables are required for the model, which indicates that also the fine structure of the spectrum is meaningful.

7.2 Slurry Analysis

The major contribution of this thesis is in the analysis of the slurry grades from the VNIR reflectance spectra. For the first time, on-line studies of the slurry VNIR spectra are presented and the possibilities for the VNIR-based assaying are investigated. The analysis is started with the final zinc concentrate of the Pyhäsalmi concentration plant and then extended to other slurries in both zinc and copper flotation circuits.

7.2.1 Zinc Concentrate

Initial results obtained for the VNIR reflectance spectrum analysis of the mineral slurries are reported already in Publication **I**. The spectra of slurry samples obtained from the final zinc concentrate at the Pyhäsalmi concentration plant were measured in laboratory and compared to the froth spectra obtained during the sample collection. The slurry spectra are detected to strongly resemble the froth spectra, which indicates that also the slurry spectrum can be used to measure the grades.

Publication **II** describes the actual combination of on-line spectral measurements of the slurry with XRF assays. The results presented in the publication form one of the key contributions of the thesis: The VNIR reflectance spectrum of the zinc concentrate slurry is shown to provide the information required for accurate prediction of the elemental grades. This forms the basis on which the work in the following publications (**III**–**VII**) is founded. Additionally, as reviewed in Section 4.2, scientific reports presenting proper applications of VNIR spectrographs to the on-line analysis of mineral flotation slurries have not been published before.

At the same time, the measurement principle where slurry is flowing through a jet flow cell and the VNIR reflectance spectrum is acquired through the cell window is demonstrated to work. Publication **II** also illustrates the necessity for updating the calibration model; the prediction ability of a static PLS model is very good for a fixed data set where every other sample is used for estimation and every other for validation, but the model quickly degrades after the estimation data period. The adaptive updating is realized by recursive PLS calibration, which suits well for the task: the modeling and prediction can be performed on-line, and the predictions obtained are even more precise.

The VNIR assaying for the typically small copper contents of the zinc concentrate slurry is improved in Publications **III** and **IV**. As discussed in Section 6.6.1, the main contribution in these two publications consists of the two new local modeling

algorithms which are designed to store the process failure information even though the model is continuously updated with new data. The algorithms clearly improve the accuracy of the VNIR assay in the case of sudden increases of the copper content, while the performance during normal operation remains at the same level as with the regular rPLS model. The importance of the result is that it enables the rapid detection of process failures, which should be dealt with as soon as possible to prevent financial losses in the form of reduced concentrate quality or valuable minerals lost in the tailings.

7.2.2 Other Slurry Lines

The analysis was augmented to other slurry lines at Pyhäsalmi by the installation of the second slurry analyzer prototype. The resulting comparison of the VNIR spectra properties and assay performance in the most important slurry lines of both zinc and copper circuits is presented in Publication **V**. The major differences of the average slurry contents between the lines are clearly seen in the average spectra of the analyzed slurries. Especially the zinc and copper concentrates have distinguished average spectra which are dominated by the optical properties of sphalerite and chalcopyrite, respectively.

The precision of the VNIR measurement in different lines was measured by calculating the coefficient of determination between the VNIR and XRF measurements. As expected, the best results are obtained for the zinc and copper concentrate slurries, where the relevant minerals (i.e. sphalerite and chalcopyrite) form the majority of the solids. The pyrite-rich tailings are more difficult to assay from the VNIR spectra, and only the iron and zinc contents of the copper middlings tailing are captured with a good precision.

7.3 Applications

The results discussed in the previous section indicate that the flotation concentrate slurries in both zinc and copper circuits of the Pyhäsalmi concentration plant can be assayed by the VNIR reflectance spectroscopy. The exploitation of the developed VNIR measurement is reported partly in all the related publications and is summarized in this section.

7.3.1 High-Frequency Assays

An advantage of the reflectance spectroscopy is the fast sampling of the spectra as opposed to the XRF analyzer with a sampling interval of around 10–20 minutes. The froth and slurry VNIR spectra were sampled every five to ten seconds in all the measurements of this work, which together with the up-to-date calibration model enabled the calculation of the high-frequency assay. Already in Publication **I** the froth is assayed from the dense VNIR measurements in order to fill in the gaps between the

sparse XRF analyses. However, a proper high-frequency assay of the zinc concentrate was obtained by the slurry analysis reported in Publication **II**.

Figure 7.1 reproduces the high-frequency assay results of the final zinc concentrate for iron, copper and zinc grades from Publication **II**. The XRF sampling frequency was doubled during the data collection, so that every other XRF sample could be saved for validation purposes. The rPLS model was updated using the estimation XRF samples, and the latest model was used for calculating the high-frequency VNIR assay on-line. A sliding 30-second average of the VNIR spectrum samples was calculated after every VNIR sample in order to mimic the 30 second long sampling of the XRF analyzer. As a result, the unfiltered VNIR assay in Figure 7.1 estimates the XRF analyzer with an interval of ten seconds.

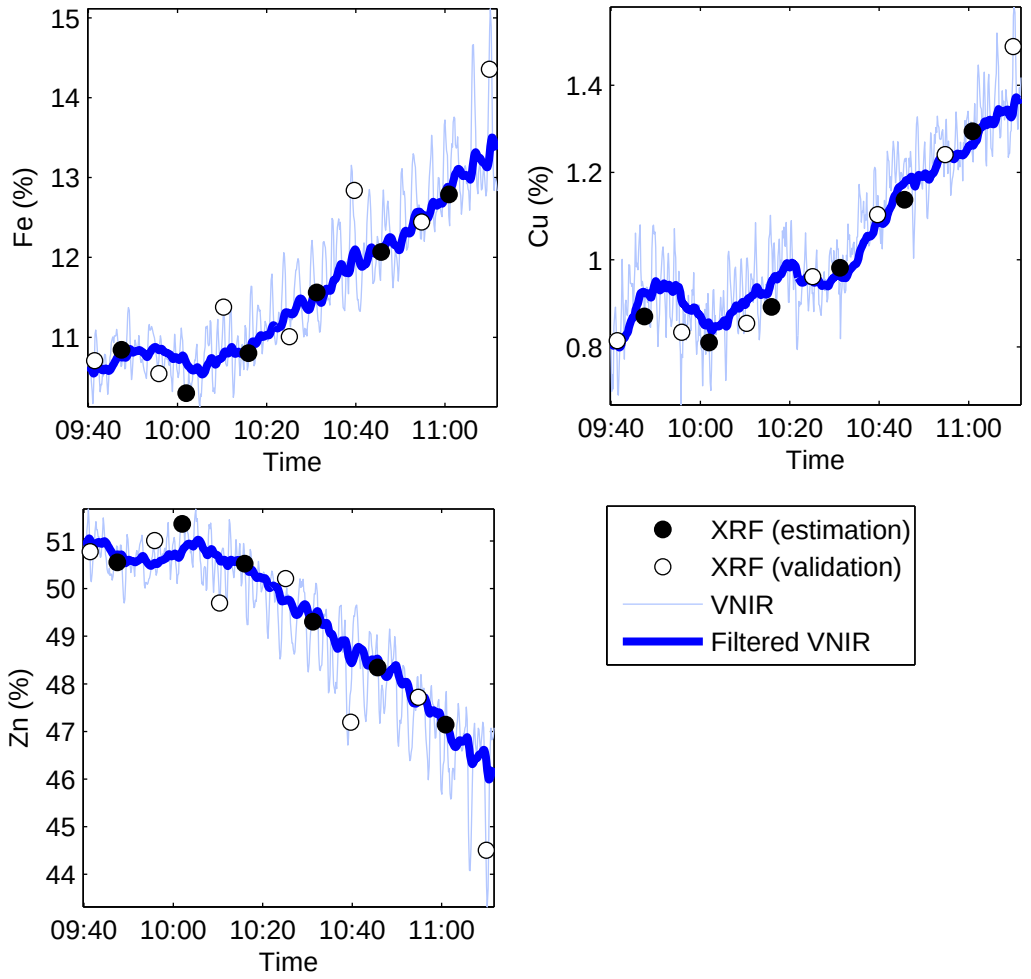

Figure 7.1: The high-frequency VNIR assay of iron, copper and zinc contents of the final zinc concentrate for a short time period. Also the low-pass filtered assay and the XRF data are shown. (Reproduced from Publication **II**)

The main observation that can be derived from the obtained high-frequency assay is that the elemental contents of the slurry at Pyhäsalmi can contain significantly large

short term changes that cannot be detected by the XRF analyzer alone. During the period illustrated in Figure 7.1, a major zinc grade drop takes place. However, the high-frequency peak-to-peak amplitude of the zinc grade is as large as two percentage points. Based on this result, the following observations can be derived:

- Accurate synchronization of the XRF and VNIR sampling is crucial to obtain reliable data for multivariate regression calculation. As demonstrated in Publication **II**, already a temporal difference of 20 seconds between the two sampling methods significantly decreases the modeling performance.
- XRF analyzer assay is only an instantaneous sample of the slurry grade, and thus does not necessarily accurately match with the more averaged slurry contents. The low-pass filtered VNIR assay, on the other hand, captures the longer term grade changes reliably.
- The discussion about the deficient sampling in froth VNIR analysis (Section 7.1 and Publication **I**) is supported by the slurry results. A more precise calibration sampling would most probably improve the accuracy of the froth VNIR analysis as well.

The two local modeling structures developed in Publications **III** and **IV** for detecting the sudden increases of small slurry grades could also be used to produce the high-frequency slurry assay. This capability is demonstrated in Publication **IV**, where the sharp increase of the final zinc concentrate copper grade is detected from the high-frequency assay before the following XRF measurement.

The analysis was further extended to the final copper concentrate slurry line in Publication **V**, where the usability of the high-frequency assay is demonstrated in the case of sudden grade drops and rapid grade oscillations. The latter case (see Figure 7.2) led to a full-scale study of signal oscillations in the Pyhäsalmi copper flotation circuit, as reported in Publication **VI**. A summary of the results is given in the next section.

Even though the high-frequency assay could readily be utilized in automatic process control, in this thesis the main emphasis is on providing the improved grade information for the process operators. To evaluate the momentarily accuracy of the measurement, an on-line estimate of the VNIR assay error distribution was developed (Publication **VII**). The basic idea is to compare the VNIR assays calculated by a set of previous PLS models to the new XRF sample before each updating step. From this data, an estimate for the VNIR assay error distribution as a function of the PLS model age is obtained. From the error distribution it is easy to compute, for example, the confidence limits for the VNIR estimate.

As a result of the work described in this thesis, the high-frequency VNIR assays of the most important elements (zinc, copper and iron) of the final copper and zinc concentrate slurries are in continuous use at the Pyhäsalmi concentration plant. The assays are available for the process operators on the automation system screens together with the corresponding XRF measurements. In addition, color-coded arrow displays illustrating the current change in the slurry grades are visible on the screens as demonstrated in Publication **VII**. Feedback from the operators indicates that the

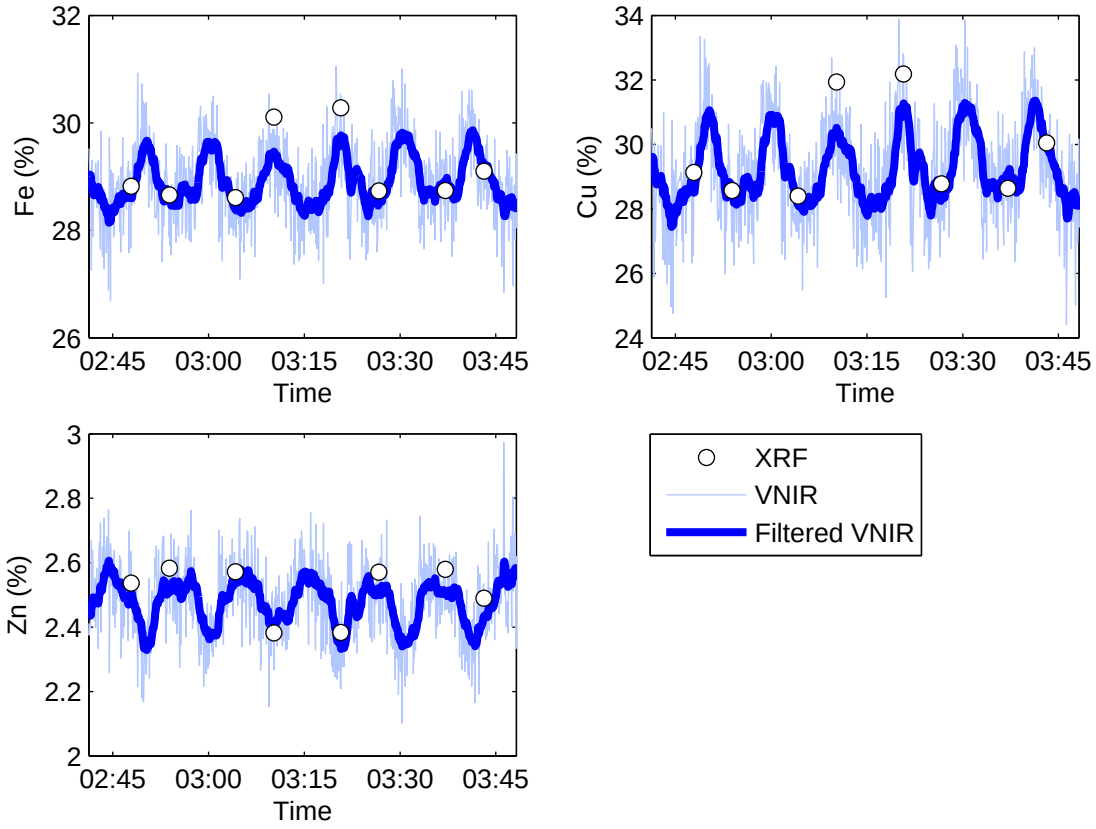

Figure 7.2: The high-frequency VNIR assay reveals well the grade oscillations in the final copper concentrate. (Reproduced from the data used in Publication **V**)

most important benefit of the new assay is the reduced sampling interval: for example, the high-frequency assay shows the response to manual control actions more rapidly than the XRF analyzer.

7.3.2 Oscillation Detection

The VNIR assay of the slurries enables for the first time the high-frequency on-line analysis of concentrate grades. As shown in Section 7.3.1 and by the results of Publications **II**, **V** and **VII**, the concentrate grades may occasionally contain oscillations on varying frequencies. In general, oscillations in industrial processes reduce the process performance and indicate that the process is not optimally controlled. In Publication **VI**, the applicability of the high-frequency VNIR assay is demonstrated by analyzing the oscillations detected in the copper assay of the final copper concentrate. The target of the research is to pinpoint the cause of the oscillations and to return the process back to steady operation.

The oscillatory analysis was based on the rSSA algorithm which estimates the on-line structure of the process signals. The results show that during the oscillations, structurally the most similar signal to the final copper grade is the flow rate of the

final concentrate. However, the same oscillatory structure is found also in other parts of the process. The most probable cause is narrowed down to the level control of the second cleaner stage, where the oscillating slurry level causes periodical grade changes to the feed of the final cleaner stage. Moreover, the oscillations are transmitted to other parts of the circuit by the tailing slurry feedbacks.

Chapter 8

Conclusions

This thesis focused on the application of VNIR reflectance spectroscopy to the analysis of mineral flotation froths and slurries. The main objective was to determine if the reflectance spectral information could be used to improve the elemental assaying of the flotation slurries. Mineral flotation is one of the most commonly used concentration methods, and the analyses of the slurry contents in the different parts of the process form the basis for the monitoring and controlling of a flotation plant.

Initially, VNIR spectra of the froth in a final zinc concentrate cell were measured and a data-based model was estimated to connect the spectra to the elemental contents of the final zinc concentrate slurry. The model was able to predict the elemental contents, and slightly better results were obtained with the VNIR measurements than with the RGB data obtained from the froth camera. However, the later study of the slurry VNIR spectra indicated that more accurate modeling would be possible if the quality of the calibration samples could be improved.

The main contributions of the thesis were obtained from the VNIR reflectance spectrum analysis of the flotation slurries. Several on-line measurement device prototypes were developed during the work, and it was shown that in the studied copper-zinc flotation process the VNIR spectra of the concentrate slurries accurately correlate with the elemental contents. Since the VNIR spectra can easily be measured with a short sampling interval (five to ten seconds) as compared to the XRF analyzer, where the sampling interval is around 15 minutes, the assay interval of the slurries can be radically reduced by predicting the elemental contents from the VNIR spectra.

It was detected, however, that a fixed calibration model does not adequately capture the changes in the slurries for longer time periods. Instead, adaptive updating of a recursive PLS model with the XRF measurements was necessary in order to utilize the spectral measurement in real process applications. As a result, the developed VNIR slurry analyzer uses both VNIR and XRF measurements to generate a high-frequency slurry assay. The disadvantage of the adaptive calibration is that the VNIR measurement is not capable of operating on its own for longer periods of time. On the other hand, the advantage is that the assay is robust to even large variations in the mineralogy, particle size distribution and other properties of the processed ore which typically hinder the analysis of flotation processes.

Additionally, the suitability of the VNIR measurement for the most important slurries at the copper-zinc flotation plant was investigated. It was shown that the tailing slurries with small valuable mineral concentrations are more difficult to analyze because of the small changes in the slurry color. Expanding the analysis range to longer wavelengths (e.g. the whole NIR range) could improve the results in small concentrations.

During the thesis work, two novel algorithms utilizing local modeling were developed. The algorithms were designed to capture sudden increases in small copper contents of the final zinc concentrate. The sudden changes in the slurry contents typically indicate a process disturbance, which should be detected as soon as possible to prevent the loss of valuable minerals. The algorithms combine recursive updating of the regression model with longer-term memory of the exceptional grade levels. It was shown that they improve the detection of the process failures with respect to the standard recursive PLS algorithm.

The high-frequency assay of the copper and zinc concentrates developed in this thesis reveals for the first time how the grades behave between the sparse XRF measurements. Surprisingly large and rapid variations were detected in both concentrates, which explains the need for accurate synchronization of the XRF and VNIR measurements. The variations also indicate that the XRF samples do not necessarily represent the average slurry grades as well as the low-pass filtered VNIR assay does.

The VNIR slurry assays were demonstrated to accurately reveal sudden grade changes and oscillations of the concentrate grades. Especially faster oscillations that would be completely missed by the XRF analyzer because of the long sampling interval can be measured by the new assay. The application of the VNIR assay to oscillation analysis was demonstrated in the thesis by a study of the plant-wide oscillations detected in the copper circuit. For this purpose, a novel on-line algorithm based on the singular spectrum analysis was developed. The oscillations visible in the final copper concentrate grade were traced to the oscillating level of one of the cleaner cell banks. Such oscillations are typically caused by poorly tuned unit controllers or by malfunctioning process equipment, and they may disturb the optimal control of the processes.

Analysis of other minerals than the ones present in the copper-zinc ore of Pyhäsalmi were beyond the scope of this work. However, the developed VNIR measurement system and the analysis methods are applicable to other flotation processes as well. Even though the laboratory spectra of the studied minerals did not show any clear absorption bands in the VNIR range, the VNIR assay was shown to work adequately in the case of the Pyhäsalmi ore. This suggests that a wide variety of other minerals could be detected by the same method as well.

In addition to the extension of the reflectance spectral analysis to other mineral types, also the utilization of a broader wavelength range would be an interesting future research objective. Especially the spectra over the whole NIR range would certainly contain more information than the narrower VNIR range applied in the thesis. Furthermore, a proper study should be conducted on the effect of the particle size distribution on the shape of the reflectance spectra.

More generally, the results of this thesis show that reflectance spectroscopy definitely is a promising measurement technique for analyzing mineral flotation froths and slurries also in real process environment. The advantages of the approach are relatively easy sample preparation and low cost of the equipment combined with the fast measurement process. On the other hand, the effect of varying slurry properties on the spectra hinders the analysis and decreases the long-term performance of an independent VNIR analysis. However, with a proper adaptive calibration, the spectra can be interpreted correctly to produce an accurate prediction of the changes in the target contents.

Bibliography

Aikio, M. (2001). Hyperspectral prism-grating-prism imaging spectrograph. VTT Publications 435, Technical Research Centre of Finland.

Aldrich, C. and Barkhuizen, M. (2003). Process system identification strategies based on the use of singular spectrum analysis. *Miner. Eng.*, 16(9):815–826.

Anderson, C. A. (1999). Direct orthogonalization. *Chemom. Intell. Lab. Syst.*, 47:51–63.

Anderson, T. W. (2003). *An Introduction to Multivariate Statistical Analysis*. Wiley Series in Probability and Statistics. John Wiley & Sons, Hoboken, New Jersey, third edition.

Atkeson, C. G., Moore, A. W., and Schaal, S. (1997). Locally weighted learning. *Artif. Intell. Rev.*, 11(1–5):11–73.

Baldridge, A. M., Hook, S. J., Grove, C. I., and Rivera, G. (2009). The ASTER spectral library version 2.0. *Remote Sens. Env.*, 113(4):711–715.

Barakat, N. A. M., Jiang, J.-H., Liang, Y.-Z., and Yu, R.-Q. (2004). Piece-wise quasi-linear modeling in QSAR and analytical calibration based on linear substructures detected by genetic algorithm. *Chemom. Intell. Lab. Syst.*, 72(1):73–82.

Bartolacci, G., Pelletier Jr., P., Tessier Jr., J., Duchesne, C., Bossé, P.-A., and Fournier, J. (2006). Application of numerical image analysis to process diagnosis and physical parameter measurement in mineral processes — Part I: Flotation control based on froth textural characteristics. *Miner. Eng.*, 19(6–8):734–747.

Basilevsky, A. (1994). *Statistical Factor Analysis and Related Methods: Theory and Applications*. Wiley Series in Propability and Mathematical Statistics. John Wiley & Sons, New York.

Bell III, J. F., Campbell, B. A., and Robinson, M. S. (1999). Planetary geology. In Rencz, A. N., editor, *Manual of Remote Sensing*, volume 3, chapter 10, pages 509–563. John Wiley and Sons, New York.

Bjørsvik, H.-R. and Martens, H. (2008). Data analysis: Calibration of NIR instruments by PLS regression. In Burns, D. A. and Ciurczak, E. W., editors, *Handbook of Near-Infrared Analysis*, pages 189–205. CRC Press, Boca Raton, third edition.

Blue Cube Systems Ltd (2009). Case study: Minerals processing, froth flotation. http://www.bluecube.co.za/site/media/090319_Northam_Article.pdf.

Bonifazi, G., Serranti, S., Volpe, F., and Zuco, R. (1998). Flotation froth characterisation by optical-digital sectioning techniques. In *Proc. Int. Conf. on Quality Control by Artificial Vision*, Takamatsu, Kagawa, Japan.

Braden, T. F., Kongas, M., and Saloheimo, K. (2002). On-line composition analysis of mineral slurries. In Mular, A. L., Halbe, D., and Barrett, D. J., editors, *Mineral Processing Plant Design, Practice and Control*, pages 2020–2047. SME, Littleton, Colorado.

Broomhead, D. S. and King, G. P. (1986). Extracting qualitative dynamics from experimental data. *Physica D*, 20(2–3):217–236.

Burns, R. G., editor (1993). *Mineralogical Applications of Crystal Field Theory*, volume 5 of *Cambridge Topics in Mineral Physics and Chemistry*. Cambridge University Press, Cambridge, 2nd edition.

Campbell, J. B., editor (2006). *Introduction to Remote Sensing*. Taylor & Francis, London and New York, 4th edition.

Carroll, J. D., Green, P. E., and Chaturvedi, A. (1997). *Mathematical Tools for Applied Multivariate Analysis*. Academic Press, San Diego.

Casali, A., Gonzales, G., Vallebuona, G., Perez, C., and Vargas, R. (2001). Grindability soft-sensors based on lithological composition and on-line measurements. *Miner. Eng.*, 14(7):689–700.

Chau, T. T. (2009). A review of techniques for measurement of contact angles and their applicability on mineral surfaces. *Miner. Eng.*, 22(3):213–219.

Ciani, A., Goss, K.-U., and Schwarzenbach, R. P. (2005). Light penetration in soil and particulate minerals. *Eur. J. Soil Sci.*, 56(5):561–574.

Cipriano, A., Guarini, M., Vidal, R., Soto, A., Sepulveda, C., Mery, D., and Briseno, H. (1998). A real time visual sensor for supervision of flotation cells. *Miner. Eng.*, 11(6):489–499.

Clark, R. N. (1999). Spectroscopy of rocks and minerals, and principles of spectroscopy. In Rencz, A. N., editor, *Manual of Remote Sensing*, volume 3, chapter 1, pages 3–58. John Wiley and Sons, New York.

Cleveland, W. S. (1979). Robust locally weighted regression and smoothing scatterplots. *J. of Am. Stat. Assoc.*, 74(369):829–836.

Cloutis, E. A., Craig, M. A., Kruzelecky, R. V., Jamroz, W. R., Scott, A., Hawthorne, F. C., and Mertzman, S. A. (2008). Spectral reflectance properties of minerals exposed to simulated Mars surface conditions. *Icarus*, 195(1):140–168.

Cooper, H. R. (1976). On-stream X-ray analysis. In Fuerstenau, M. C., editor, *Flotation, A. M. Gaudin Memorial Volume*, volume 2, pages 865–894. American Institute of Mining, Metallurgical and Petroleum Engineers, Inc., New York.

Crozier, R. D., editor (1992). *Flotation: Theory, Reagents and Ore Testing*. Pergamon Press, Oxford.

D'Amico, A., Di Natale, C., Lo Castro, F., Iarossi, S., Catini, A., and Martinelli, E. (2009). Volatile compounds detection by IR acousto-optic detectors. In Byrnes, J., editor, *Unexploded Ordnance Detection and Mitigation*, NATO Science for Peace and Security Series B: Physics and Biophysics, pages 21–60. Springer, Dordrecht, The Netherlands.

Davies, A. M. C., Britcher, H. V., Franklin, J. G., Ring, S. M., Grant, A., and McClure, W. G. (1988). The application of fourier-transformed near-infrared spectra to quantitative analysis by comparison of similarity indices (CARNAC). *Mikrochim. Acta*, 94(1–6):61–64.

Davies, T. and Fearn, T. (2008). Local methods and CARNAC-D. In Burns, D. A. and Ciurczak, E. W., editors, *Handbook of Near-Infrared Analysis*, pages 781–795. CRC Press, Boca Raton, third edition.

Dayal, B. S. and MacGregor, J. F. (1997a). Improved PLS algorithms. *J. Chemom.*, 11(1):73–85.

Dayal, B. S. and MacGregor, J. F. (1997b). Recursive exponentially weighted PLS and its applications to adaptive control and prediction. *J. Process Control*, 7(3):169–179.

De Jong, S. and Ter Braak, C. J. F. (1994). Comments on the PLS kernel algorithm. *J. Chemom.*, 8(2):169–174.

De Waal, P. (2007). Tomorrow's technology — out of Africa — today. In *Proc. of The Fourth Southern African Conference on Base Metals 2007*, Swakopmund, Namibia. Southern African Institute of Mining and Metallurgy.

De Waal, P. and Du Plessis, F. E. (2005). Automatic control of a high tension roll separator. In Akser, M. and Elder, J., editors, *Heavy Minerals Conf. Proc. 2005*, pages 241–249, Florida. Society of Mining, Metallurgy, and Exploration.

Englert, A. H., Krasowska, M., Fornasiero, D., Ralston, J., and Rubio, J. (2009). Interaction force between an air bubble and a hydrophilic spherical particle in water, measured by the colloid probe technique. *Int. J. Miner. Process.*, 92(3–4):121–127.

Erdogmus, D., Rao, Y. N., Peddaneni, H., Hedge, A., and Principe, J. C. (2004). Recursive principal components analysis using eigenvector matrix perturbation. *EURASIP J. Appl. Signal Process.*, 2004(13):2034–2041.

Fearn, T. (2000). On orthogonal signal correction. *Chemom. Intell. Lab. Syst.*, 50:47–52.

Fearn, T. and Davies, A. M. C. (2003). Locally-biased regression. *J. Near Infrared Spectrosc.*, 11(6):467–478.

Fearn, T., Riccioli, C., Garrio-Varo, A., and Guerrero-Ginel, J. E. (2009). On the geometry of SNV and MSC. *Chemom. Intell. Lab. Syst.*, 96(1):22–26.

Flintoff, B. C. (1992). Measurement issues in quality "control". In *Proc. of the 1992 Toronto CMP Branch Meeting*, Toronto, Canada.

Fornasier, S., Migliorini, A., Dotto, E., and Barucci, M. A. (2008). Visible and near infrared spectorscopic investigation of E-type asteroids, including 2867 Steins, a target of the Rosetta mission. *Icarus*, 196(1):119–134.

Fuerstenau, M. C., Jameson, G. J., and Yoon, R.-H., editors (2007). *Froth Flotation: A Century of Innovation*. Society of Mining Metallurgy & Exploration.

Gebhardt, J. E., Tolley, W. K., and Ahn, J. H. (1993). Color measurements of minerals and mineralized froths. *Min. & Metall. Process.*, 10(2):96–99.

Geladi, P. and Kowalski, B. R. (1986). Partial least-squares regression: A tutorial. *Anal. Chim. Acta*, 185:1–17.

Geladi, P., MacDougall, D., and Martens, H. (1985). Linearization and scatter-correction for near-infrared reflectance spectra of meat. *Applied Spectrosc.*, 39(3):491–500.

Gemperline, P., editor (2006). *Practical Guide to Chemometrics*. CRC Press, Boca Raton, FL, second edition.

Glen, W. G., Dunn III, W. J., and Scott, D. R. (1989a). Principal components analysis and partial least squares regression. *Tetrahedron Comput. Methodol.*, 2(6):349–376.

Glen, W. G., Sarker, M., Dunn III, W. J., and Scott, D. R. (1989b). UNIPALS: Software for principal components analysis and partial least squares regression. *Tetrahedron Comput. Methodol.*, 2(6):377–396.

Goetz, A. F. H. (2009). Three decades of hyperspectral remote sensing of the earth: A personal view. *Remote Sens. Env.*, 113:S5–S16.

Goetz, A. F. H., Curtiss, B., and Shiley, D. A. (2009). Rapid gangue mineral concentration measurement over conveyors by NIR reflectance spectroscopy. *Miner. Eng.*, 22(5):490–499.

Golyandina, N., Nekrutkin, V., and Zhigljavsky, A. (2001). *Analysis of Time Series Structure: SSA and Related Techniques*. Number 90 in Monographs on Statistics and Applied Probability. Chapman & Hall/CRC, Boca Raton.

Gorain, B. K., Oravainen, H., Allenius, H., Peaker, R., Weber, A., and Tracyzk, F. (2007). Mechanical froth flotation cells. In Fuerstenau, M. C., Jameson, G. J., and Yoon, R.-H., editors, *Froth Flotation: A Century of Innovation*, pages 637–680. Society of Mining Metallurgy & Exploration.

Griffiths, P. R. and Dahm, D. J. (2008). Continuum and discontinuum theories of diffuse reflection. In Burns, D. A. and Ciurczak, E. W., editors, *Handbook of Near-Infrared Analysis*, pages 21–64. CRC Press, Boca Raton, third edition.

Guyot, O., Monredon, T., LaRosa, D., and Broussaud, A. (2004). VisioRock, an integrated vision technology for advanced control of comminution circuits. *Miner. Eng.*, 17(11–12):1227–1235.

Hägglund, T. (1995). A control-loop performance monitor. *Control Eng. Pract.*, 3(11):1543–1551.

Hapke, B. (2005). *Theory of Reflectance and Emittance Spectroscopy*, volume 3 of *Topics in remote sensing*. Cambridge University Press, Cambridge, UK, 1st paperback edition.

Hargrave, J. M. and Hall, S. T. (1997). Diagnosis of concentrate grade and mass flowrate in tin flotation from colour and surface texture analysis. *Miner. Eng.*, 10(6):613–621.

Hargrave, J. M., Miles, N. J., and Hall, S. T. (1996). The use of grey level measurement in predicting coal flotation performance. *Miner. Eng.*, 9(6):667–674.

Hassani, H., Heravi, S., and Zhigljavsky, A. (2009). Forecasting European industrial production with singular spectrum analysis. *Int. J. Forecast.*, 25(1):103–118.

Hätönen, J. (1999). Image analysis in mineral flotation. Technical Report 116, Helsinki University of Technology, Control Engineering Laboratory.

Helland, K., Berntsen, H. E., Borgen, O. S., and Martens, H. (1991). Recursive algorithm for partial least squares regression. *Chemom. Intell. Lab. Syst.*, 14:129–137.

Hindle, P. H. (2008). Historical development. In Burns, D. A. and Ciurczak, E. W., editors, *Handbook of Near-Infrared Analysis*, pages 3–6. CRC Press, Boca Raton, third edition.

Hoerl, A. E. and Kennard, R. W. (1970). Ridge regression: Biased estimation for nonorthogonal problems. *Technometrics*, 12(1):55–67.

Holtham, P. N. and Nguyen, K. K. (2002). On-line analysis of froth surface in coal and mineral flotation using JKFrothCam. *Int. J. Miner. Process.*, 64:163–180.

Hook, S. J., Abbott, E. A., Grove, C., Kahle, A. B., and Palluconi, F. (1999). Use of multispectral thermal infrared data in geological studies. In Rencz, A. N., editor, *Manual of Remote Sensing*, volume 3, chapter 2, pages 59–110. John Wiley and Sons, New York.

Höskuldsson, A. (1988). PLS regression methods. *J. Chemom.*, 2(3):211–228.

Hyötyniemi, H. (2001). Multivariate regression — techniques and tools. Technical Report 125, Helsinki University of Technology, Control Engineering Laboratory.

Ingle Jr., J. D. and Crouch, S. R. (1988). *Spectrochemical Analysis*. Prentice-Hall International, Inc.

Inmet Mining Corporation (2008). Pyhäsalmi Mine. brochure.

Inmet Mining Corporation (2009). Annual Review 2008. pages A14–A15, `http://www.inmetmining.com/Theme/Inmet/files/pdf/annual%20report.pdf`.

Jackson, J. E. (2003). *A User's Guide to Principal Components*. John Wiley Series in Probability and Statistics. John Wiley & Sons, Hoboken, New Jersey.

Jemwa, G. T. and Aldrich, C. (2006). Classification of process dynamics with Monte Carlo singular spectrum analysis. *Comput. Chem. Eng.*, 30(15):816–831.

Kaartinen, J. (2001). Data acquisition and analysis system for mineral flotation. Technical Report 126, Helsinki University of Technology, Control Engineering Laboratory.

Kaartinen, J., Haavisto, O., and Hyötyniemi, H. (2006a). On-line colour measurement of flotation froth. In *Proc. of The Ninth IASTED Int. Conf. on Intelligent Systems and Control (ISC 2006), Honolulu, Hawaii, USA*, pages 164–169.

Kaartinen, J., Hätönen, J., Hyötyniemi, H., and Miettunen, J. (2006b). Machine-vision-based control of zinc flotation – a case study. *Control Eng. Pract.*, 14:1455–1466.

Khan, S. D. and Mahmood, K. (2008). The application of remote sensing techniques to the study of ophiolites. *Earth-Sci. Rev.*, 89(3–4):135–143.

Kracht, W. and Finch, J. A. (2009). Bubble break-up and the role of frother and salt. *Int. J. Miner. Process.*, 92(3–4):153–161.

Kruse, F. A. (1996). Identification and mapping of minerals in drill core using hyperspectral image analysis of infrared reflectance spectra. *Int. J. Rem. Sens.*, 17(9):1623–1632.

Kumaresan, R. and Tufts, D. W. (1980). Data-adaptive principal component signal processing. In *Proc. of the 19th IEEE Conf. on Decision and Control*, volume 19, pages 949–954.

Laurila, H., Karesvuori, J., and Tiili, O. (2002). Strategies for instrumentation and control of flotation circuits. In Mular, A. L., Halbe, D. N., and Barrat, D. J., editors, *Mineral Processing Plant Design, Practice and Control*, volume 2, pages 2174–2195. Society for Mining, Metallurgy, and Exploration.

Li, W., Yue, H. H., Valle-Cervantes, S., and Qin, S. J. (2000). Recursive PCA for adaptive process monitoring. *J. Process Control*, 10(5):471–486.

Lindgren, F., Geladi, P., and Wold, S. (1993). The kernel algorithm for PLS. *J. Chemom.*, 7(1):45–59.

Lindgren, F. and Rännar, S. (1998). Alternative partial least squares (PLS) algorithms. *Perspectives in Drug Discov. and Des.*, 12–14:105–113.

Liu, J. J. and MacGregor, J. F. (2008). Froth-based modeling and control of flotation processes. *Miner. Eng.*, 21(9):642–651.

Liu, J. J., MacGregor, J. F., Duchesne, C., and Bartolacci, G. (2005). Flotation froth monitoring using multiresolutional multivariate image analysis. *Miner. Eng.*, 18(1):65–76.

Ljung, L. (1999). *System Identification, Theory for the User*. Prentice Hall PTR, Upper Saddle River, NJ, 2 edition.

Ljung, L. and Söderström, T. (1983). *Theory and Practice of Recursive Identification*. MIT Press, Cambridge, MIT.

Marrelli, L., Bilato, R., Franz, P., Martin, P., Murari, A., and O'Gorman, M. (2001). Singular spectrum analysis as a tool for plasma fluctuations analysis. *Rev. Sci. Instrum.*, 72(1):499–502.

Marschallinger, R. (1997). Automatic mineral classification in the macroscopic scale. *Comput. & Geosci.*, 23(1):119–126.

Martens, H. and Næs, T. (1989). *Multivariate Calibration*. John Wiley & Sons.

Matis, K. A. and Zouboulis, A. I. (1995). An overview of the process. In Matis, K. A., editor, *Flotation Science and Engineering*, pages 1–44. Marcel Dekker, Inc., New York.

Mauger, A. J. and Huntington, J. F. (2005). Hylogging applications in exploration. In *Proc. of the Mineral Exploration Through Cover 2005, Abstract Volume*, pages 20–21, Mawson laboratories, University of Adelaide.

McKee, D. J. (1991). Automatic flotation control - a review of 20 years of effort. *Miner. Eng.*, 4(7–11):653–666.

Mendez, D. A., Gálvez, E. D., and Cisternas, L. A. (2009). State of the art in the conceptual design of flotation circuits. *Int. J. Miner. Process.*, 90(1–4):1–15.

Miletic, I., Quinn, S., Dudzic, M., Vaculik, V., and Champagne, M. (2004). An industrial perspective on implementing on-line applications of multivariate statistics. *J. Process Control*, 14(8):821–836.

Moolman, D. W., Aldrich, C., and Van Deventer, J. S. J. (1994). Digital image processing as a tool for on-line monitoring of froth in flotation plants. *Miner. Eng.*, 7(9):1149–1164.

Moolman, D. W., Aldrich, C., and Van Deventer, J. S. J. (1995). The monitoring of froth surfaces on industrial flotation plants using connectionist image processing techniques. *Miner. Eng.*, 8(1/2):23–30.

Morar, S. H., Forbes, G., Heinrich, G. S., Bradshaw, D. J., King, D., Adair, B. J. I., and Esdaile, L. (2005). The use of a colour parameter in a machine vision system, SmartFroth, to evaluate copper floation performance at Rio Tinto's Kennecot copper concentrator. In Jameson, G. J., editor, *Centenary of Flotation Symposium, Brisbane, Australia, 6–9 June 2005 - Proceedings*, pages 147–152. The Australasian Institute of Mining and Metallurgy.

Murray-Smith, R. and Johansen, T. A. (1997). *Multiple Model Approaches to Modeling and Control*. Taylor & Francis, London.

Naes, T. and Isaksson, T. (1991). Splitting of calibration data by cluster analysis. *J. Chemom.*, 5(1):49–65.

Naes, T. and Isaksson, T. (1992). Locally weighted regression in diffuse near-infrared transmittance spectroscopy. *Appl. Spectrosc.*, 46(1).

Norris, K. H. (1983). Multivariate analysis of raw materials. In Shemilt, L. W., editor, *Chemistry and World Food Supplies: the New Frontiers, Chemraw II*, pages 527–535. Pergamon Press.

Oestreich, J. M., Tolley, W. K., and Rice, D. A. (1995). The development of a color sensor system to measure mineral compositions. *Miner. Eng.*, 8(1/2):31–39.

Osborne, B. G., Fearn, T., and Hindle, P. H. (1993). *Practical NIR Spectroscopy with Applications in Food and Beverage Analysis*. Longman Publishing Group, Harlow, 2nd edition.

Pérez-Marín, D., Garrido-Varo, A., and Guerrero, J. (2007). Non-linear regression methods in NIRS quantitative analysis. *Talanta*, 72(1):28–42.

Pietilä, J. and Haavisto, O. (2009). Reflectance spectroscopy based classification of ore. In *Preprints of the Workshop on Automation in Mining, Mineral and Metal Industry*, Viña del Mar, Chile. accepted.

Qin, S. J. (1993). Partial least squares regression for recursive system identification. In *Proc. of the 32nd Conf. on Decision and Control, San Antonio, Texas*, pages 2617–2622.

Qin, S. J. (1998). Recursive PLS algorithms for adaptive data modeling. *Comput. Chem. Eng.*, 22(4/5):503–514.

Rännar, S., Lindgren, F., Geladi, P., and Wold, S. (1994). A PLS kernel algorithm for data sets with many variables and fewer objects. Part 1: Theory and algorithm. *J. Chemom.*, 8(2):111–125.

Rännar, S., Lindgren, F., Geladi, P., and Wold, S. (1995). A PLS kernel algorithm for data sets with many variables and fewer objects. Part II: Cross-validation, missing data and examples. *J. Chemom.*, 9(6):459–470.

Rantalainen, M., Bylesjö, M., Cloarec, O., Nicholson, J. K., Holmes, E., and Trygg, J. (2007). Kernel-based orthogonal projections to latent structures (K-OPLS). *J. Chemom.*, 21:376–385.

Rao, S. R., editor (2004). *Surface Chemistry of Froth Flotation.* Kluwer Academic/Plenum Publishes, New York, second edition.

Remes, A., Saloheimo, K., and Jämsä-Jounela, S.-L. (2007). Effect of speed and accuracy of on-line elemental analysis on flotation control performance. *Miner. Eng.*, 20(11):1055–1066.

Rencz, A. N., editor (1999). *Manual of Remote Sensing.* John Wiley and Sons, New York, 3rd edition.

Reyneke, L., du Plessis, F. E., and van der Westhuizen, G. (2003). Development and evaluation of technology for quantifying the mineral composition of process streams in the typical dry mill in the heavy mineral industry. In *Heavy Minerals Conf. Proc. 2003*, Johannesburg, South Africa. Southern African Institute of Mining and Metallurgy.

Rodó, X., Baert, E., and Comin, F. A. (1997). Variations in seasonal rainfall in Southern Europe during the present century: relationships with the North Atlantic Oscillation and the El Niño-Southern Oscillation. *Clim. Dyn.*, 13(4):275–284.

Sadr-Kazemi, N. and Cilliers, J. J. (1997). An image processing algorithm for measurement of flotation froth bubble size and shape distributions. *Miner. Eng.*, 10(10):1075–1083.

Schaal, S. and Atkeson, C. G. (1998). Constructive incremental learning from only local information. *Neural Comput.*, 10(8):2047–2084.

Shen, Q., Jiang, J.-H., Jiao, C.-X., Huan, S.-Y., Shen, G.-L., and Yu, R.-Q. (2004). Optimized partition of minimum spannin tree for piecewise modeling by particle swarm algorithm. QSAR studies of antagonism of angiotensin II antagonists. *J. Chem. Inf. Model.*, 44(6):2027–2031.

Shenk, J. S. and Westerhuis, M. O. (1997). Investigation of a LOCAL calibration procedure for near infrared instruments. *J. Near Infrared Spectrosc.*, 5(4).

Siesler, H. W. (2008). Basic principles of near-infrared spectroscopy. In Burns, D. A. and Ciurczak, E. W., editors, *Handbook of Near-Infrared Analysis*, pages 7–19. CRC Press, Boca Raton, third edition.

Sjöblom, J., Svensson, O., Josefson, M., Kullberg, H., and Wold, S. (1998). An evaluation of orthogonal signal correction applied to calibration transfer of near infrared spectra. *Chemom. Intell. Lab. Syst.*, 44:229–244.

Squire, R. J., Herrmann, Q., Pape, D., and Chalmers, D. I. (2007). Evolution of the Peak Hill high-sulfication epithermal Au-Cu deposit, eastern Australia. *Miner. Deposita*, 42(5):489–503.

Svensson, O., Kourti, T., and MacGregor, J. F. (2002). An investigation of orthogonal signal correction algorithms and their characteristics. *J. Chemom.*, 12:176–188.

Symonds, P. J. and De Jager, G. (1992). A technique for automatically segmenting images of the surface froth structures that are prevalent in industrial flotation cells. In *Proc. of the 1992 South African Symposium on Communications and Signal Processing*, pages 111–115, University of Cape Town, Rondebosch, South Africa.

Taylor, G. R. (2000). Mineral and lithology mapping of drill core pulps using visible and infrared spectrometry. *Nat. Resour. Res.*, 9(4):257–268.

Tessier, J., Duchese, C., and Bartolacci, G. (2007). A machine vision approach to on-line estimation of run-of-mine ore composition on conveyor belts. *Miner. Eng.*, 20(12):1129–1144.

Thornhill, N. F. and Hägglund, T. (1997). Detection and diagnosis of oscillations in control loops. *Control Eng. Pract.*, 5(10):1343–1354.

Thornhill, N. F., Huang, B., and Zhang, H. (2003). Detection of multiple oscillations in control loops. *J. Process Control*, 13(1):91–100.

Thornhill, N. F., Shah, S. L., Huang, B., and Vishnubhotla, B. (2002). Spectral principal component analysis of dynamic process data. *Control Eng. Pract.*, 10(8):833–846.

Trygg, J. and Wold, S. (2002). Orthogonal projections to latent structures. *Chemom. Intell. Lab. Syst.*, 16:119–128.

Trygg, J. and Wold, S. (2003). O2-PLS, a two block (X-Y) latent variable regression (LVR) method with an integral OSC filter. *J. Chemom.*, 17:53–64.

Tzagkarakis, G., Papadopouli, M., and Tsakalides, P. (2009). Trend forecasting based on Singular Spectrum Analysis of traffic workload in a large-scale wireless LAN. *Perform. Eval.*, 66(3–5):173–190.

Vautard, R. and Ghil, M. (1989). Singular spectrum analysis in nonlinear dynamics, with applications to paleoclimatic time series. *Physica D*, 35(3):395–424.

Vijayakumar, S., D'Souza, A., and Schaal, S. (2005). Incremental online learning in high dimensions. *Neural Comput.*, 17(12):2602–2634.

Wang, Z., Isaksson, T., and Kowalski, B. R. (1994). New approach for distance measurement in locally weighted regression. *Anal. Chem.*, 66(2):249–260.

Westerhuis, J. A., de Jong, S., and Smilde, A. K. (2001). Direct orthogonal signal correction. *Chemom. Intell. Lab. Syst.*, 56:13–25.

Wills, B. A. and Napier-Munn, T. (2006). *Wills' Mineral Processing Technology*. Butterworth-Heinemann, 7th edition.

Wold, H. (1965). Estimation of principal components and related models by iterative least squares. In Krishnaiah, P. R., editor, *Multivariate Analysis: Proc. Int. Symposium Held in Dayton, Ohio, June 14-19, 1965*, pages 391–420. Academic Press.

Wold, H. (1966). Nonlinear estimation by iterative least squares procedures. In David, F., editor, *Research Papers in Statistics*, pages 411–444. Wiley, London.

Wold, S., Antti, H., Lindgren, F., and Öhman, J. (1998). Orthogonal signal correction of near-infrared spectra. *Chemom. Intell. Lab. Syst.*, 44:175–185.

Wold, S., Esbensen, K., and Geladi, P. (1987). Principal component analysis. *Chemom. Intell. Lab. Syst.*, 2:37–52.

Wold, S., Martens, H., and Wold, H. (1983). The multivariate calibration problem in chemistry solved by the PLS method. In *Matrix Pencils*, pages 286–293. Springer, Berlin/Heidelberg.

Wold, S., Sjöström, M., and Eriksson, L. (2001). PLS-regression: a basic tool of chemometrics. *Chemom. Intell. Lab. Syst.*, 58:109–130.

Workman Jr., J. J. (2008). NIR spectroscopy calibration basics. In Burns, D. A. and Ciurczak, E. W., editors, *Handbook of Near-Infrared Analysis*, pages 123–150. CRC Press, Boca Raton, third edition.

Xia, C., Howell, J., and Thornhill, N. F. (2005). Detecting and isolating multiple plant-wide oscillations via spectral independent component analysis. *Automatica*, 41(12):2067–2075.

Yang, K., Lian, C., Huntington, J. F., Peng, Q., and Wang, Q. (2005). Infrared spectral reflectance characterization of the hydrothermal alteration at the Tuwu Cu-Au deposit, Xinjiang, China. *Miner. Deposita*, 40(3):324–336.

Yiou, P., Ghil, M., Jouzel, J., Paillard, D., and Vautard, R. (1994). Nonlinear variability of the climatic system from singular and power spectra of Late Quaternary records. *Clim. Dyn.*, 9(8):371–389.

HELSINKI UNIVERSITY OF TECHNOLOGY CONTROL ENGINEERING

Editor: H. Koivo

Report 150 Virtanen, T.
Fault Diagnostics and Vibration Control of Paper Winders. June 2006.

Report 151 Hyötyniemi, H.
Neocybernetics in Biological Systems. August 2006.

Report 152 Hasu, V.
Radio Resource Management in Wireless Communication: Beamforming, Transmission Power Control, and Rate Allocation. June 2007.

Report 153 Hrbček, J.
Active Control of Rotor Vibration by Model Predictive Control - A simulation study. May 2007.

Report 154 Mohamed, F. A.
Microgrid Modelling and Online Management. January 2008.

Report 155 Eriksson, L., Elmusrati, M., Pohjola, M. (eds.)
Introduction to Wireless Automation - Collected papers of the spring 2007 postgraduate seminar. April 2008.

Report 156 Korkiakoski, V.
Improving the Performance of Adaptive Optics Systems with Optimized Control Methods. April 2008.

Report 157 Al.Towati, A.
Dynamic Analysis and QFT-Based Robust Control Design of Switched-Mode Power Converters. September 2008.

Report 158 Eriksson, L.
PID Controller Design and Tuning in Networked Control Systems. October 2008.

Report 159 Pohjoranta, A.
Modelling Surfactant Mass Balance with the ALE Method on Deforming 2D Surfaces. May 2009.

Report 160 Kaartinen, J.
Machine Vision in Measurement and Control of Mineral Concentration Process. June 2009.

Report 161 Hölttä, V.
Plant Performance Evaluation in Complex Industrial Applications. September 2009.

Report 162 Halmevaara, K.
Simulation Assisted Performance Optimization of Large-Scale Multiparameter Technical Systems. September 2009.

Report 163 Haavisto, O.
Reflectance Spectrum Analysis of Mineral Flotation Froths and Slurries. November 2009.

ISBN 978-952-248-236-5
ISSN 0356-0872
Yliopistopaino, Helsinki 2009